

THESIS

EXPLORATION OF UNIQUE POROUS BONE MATERIALS FOR CANDIDACY IN  
BIOINSPIRED MATERIAL DESIGN

Submitted by

Timothy W. Seek

Department of Mechanical Engineering

In partial fulfillment of the requirements

For the Degree of Master of Science

Colorado State University

Fort Collins, Colorado

Spring 2018

Master's Committee:

Advisor: Seth Donahue

Thomas Bradley

Gregory Florant

Copyright by Timothy Seek 2018

All Rights Reserved

## ABSTRACT

### EXPLORATION OF UNIQUE POROUS BONE MATERIALS FOR CANDIDACY IN BIOINSPIRED MATERIAL DESIGN

Bioinspired material design draws inspiration for improved technologies from unique functional adaptations found in nature. Grizzly bear (*Ursus arctos horribilis*), cave bear (*Ursus spelaeus*), edmontosaur (*Edmontosaurus annectens*) (*Edmontosaurus regalis*), and bighorn sheep (*Ovis canadensis*) exhibit unique functional examples of porous bone structures. Grizzly bear trabecular bone does not lose bone density during long periods of disuse. Cave bears, being larger than grizzly bears, give a unique perspective of trabecular bone property scaling relationships in animals from the near past. Edmontosaurs were expected to have grown to gigantic sizes weighing  $7936 \pm 1991$  kg creating a unique high force loading environment in dinosaur trabecular bone. Bighorn sheep butt heads during the mating season routinely generating near 100g accelerations and approximately 3400N forces in their horn core bone during impact. Morphological trabecular bone properties of bone volume fraction (BV/TV), trabecular thickness (Tb.Th), trabecular separation (Tb.Sp), and trabecular number (Tb.N) were examined using micro-computed tomography ( $\mu$ CT) imaging for the underlying trabecular bone in the proximal tibiae of grizzly bear, cave bear, and edmontosaurus animals. Morphological bone properties were compared against body mass scaling relationships from extant mammals. Cave bear trabecular bone was found to have larger BV/TV and Tb.Th than modern grizzly bears. The larger BV/TV may indicate environmental drivers on cave bear trabecular bone properties. To our knowledge, the measurement of dinosaur trabecular bone properties is a novel

concept. Adult edmontosaur BV/TV was measured at an average greater than 60% which was significantly different from extant species BV/TV values. Additionally, adult edmontosaurus Tb.Th, and Tb.Sp were measured at comparable values to small mammals. The difference in edmontosaur BV/TV from extant mammals may be a potential clue in why extant terrestrial animals do not reach the same levels of gigantism as dinosaurs. Additionally, mimicking the continuum properties of edmontosaur trabecular bone in an engineered foam may have potential usage in optimized high strength foams. Bighorn sheep horn core bone exhibits observational and morphological properties different from typical trabecular bone in thickness, separation and number. Due to these differences, the bighorn sheep horn core bone is being considered as a new type of porous bone architecture referred to as 'velar' bone. The velar bone morphology indicates that it is highly adapted to resist high impact bending through widely separated and thick bone formations. Future bioinspired engineering foam designs mimicking the structures of porous bone outlined in this research could be useful for energy absorption in repeated high impact loading. The work presented here does not include efforts to create a bioinspired structural foam. However, this research focuses on the quantification of porous bone structural properties optimized for unique mechanical environments for the purposes of guiding future research towards structural foam design.

## ACKNOWLEDGEMENTS

I would to acknowledge my advisor, Dr. Seth Donahue, for providing mentorship and assistance throughout my master's thesis work.

I would also like to acknowledge my committee members, Dr. Thomas Bradley and Dr. Gregory Florant. In addition, I would like to acknowledge Dr. Joe Sertich and the Denver Museum of Nature and Science, Dr. Tony Fiorillo and the Perot Museum of Nature and Science, and the Colorado Department of Wildlife for providing me with samples for this research. Finally, I would like to acknowledge all of my lab-colleagues including Samantha Wojda, Jason Hinrichs, Luca Fuller, Trevor Aguirre, and Emily Mulawa for providing feedback throughout the duration of this research.

## TABLE OF CONTENTS

ABSTRACT.....	ii
ACKNOWLEDGEMENTS.....	iv
LIST OF FIGURES .....	viii
Chapter 1: Introduction.....	1
1.1 Overview of biomimicry and purpose .....	1
1.2 Bone Adaptations To Mechanical Loading .....	1
1.3 Overview of Trabecular Bone.....	8
1.4 Grizzly Bears and Cave Bears .....	11
1.4.1 Grizzly Bear and Cave Bear Hypothesis .....	12
1.5 Edmontosaurus.....	13
1.5.1 Edmontosaurus Hypothesis.....	14
1.6 Bighorn Sheep.....	14
1.6.1 Bighorn Sheep Hypothesis.....	16
Chapter 2: Methods and Results .....	17
2.1 Grizzly Bear and Cave Bear Methods and Results.....	17
2.1.1 Sample Information .....	17
2.1.2 Sample Preparation Procedures .....	17
2.1.3 Sample Measurements .....	18

2.1.4 Cave Bear and Grizzly Bear Statistics .....	20
2.1.5 Grizzly Bear and Cave Bear Trabecular Bone Morphology Results .....	21
2.2 Edmontosaur Methods and Results.....	24
2.2.1 Edmontosaur Samples.....	24
2.2.2 Edmontosaur Sample Drilling Locations.....	25
2.2.3 Edmontosaur Sample Preparation.....	26
2.2.4 Edmontosaur Sample Imaging.....	27
2.2.5 Edmontosaur Statistics.....	28
2.2.6 Edmontosaur Fossil Bone Verification.....	31
2.3 Bighorn Sheep Methods.....	35
2.3.1 Bighorn Sheep Samples .....	35
2.3.2 Bighorn Sheep Sample preparation .....	35
2.3.3 Bighorn Sheep Sample Imaging .....	35
2.3.4 MATLAB Code Formulation .....	36
2.3.5 MATLAB Code Validation .....	37
2.3.6 Bighorn Sheep horn and horn core measurements .....	37
2.3.7 Bighorn Sheep Statistics .....	39
2.3.8 Bighorn Sheep Results.....	39
Chapter 3: Discussion .....	43
3.1 Cave Bear and Grizzly Bear Discussion.....	43

3.2 Dinosaur Discussion .....	45
3.3 Bighorn Sheep Horns Discussion .....	48
References.....	52

## LIST OF FIGURES

Figure 1: Above: cortical and trabecular bone examples and locations in moose femur. Below left: a cutaway of the proximal femur of a black bear. Below right: A zoomed in view of the trabecular bone structure of a black bear femur.....	2
Figure 2: Trabecular bone morphological property diagrams. Upper left: Bone volume fraction given by total bone volume relative to total volume. Upper right: Trabecular thickness shown as the thickness of the bone formation. Lower left: Trabecular separation shown as the distance between bone formations. Lower right: Trabecular number shown as the count of bone formations over a distance. ....	4
Figure 3: Bighorn sheep skull with horn cutaway. ....	14
Figure 4: Left a cutaway of a bighorn sheep horn core revealing the sail-like bone formations within. Right: a cutaway of traditionally regarded trabecular bone from a black bear femur.....	15
Figure 5: Diagram depicting the coring setup.....	18
Figure 6: A depiction of a cave bear tibial plateau with markings indicating how the width measurements were made for the tibial plateau in red and yellow. An example of the drilling location is highlighted in blue.....	19
Figure 7: Left: grizzly bear $\mu$ CT scout view detailing evaluation region distal to the physis. Right: cave bear $\mu$ CT scout view showing evaluation region distal to the physeal scar. ....	20
Figure 8: Measured bone lengths compared between cave bears and grizzly bears.....	21
Figure 9: Plateau width and midshaft diameter measurement t-tests.. ....	22
Figure 10: Top row: 3 dimensional reconstructions of cave bear $\mu$ CT scan volumes. Bottom row: 3 dimensional reconstructions of grizzly bear $\mu$ CT scan volumes .....	23

Figure 11: Trabecular bone morphological property comparisons between cave bears and grizzly bears. ....	24
Figure 12: PET/CT radiograph scout for high and low density regions in fossils.....	26
Figure 13: Scout view of edmontosaur core and resulting 3D reconstruction.....	27
Figure 14: ANOVA of BV/TV comparing tibia BV/TV in 9 different species.....	28
Figure 15: ANOVA of Tb.Th comparing tibia Tb.Th in 8 different species.....	29
Figure 16: ANOVA of Tb.Sp comparing tibia Tb.Sp in 8 different species.. ....	30
Figure 17: ANOVA of Tb.N comparing tibia Tb.N in 6 different species.....	31
Figure 18: Example edmontosaur SEM EDS maps.....	33
Figure 19: Sheep SEM EDS maps. Left: ewe. Right: ram.....	33
Figure 20: Rock matrix SEM EDS. ....	34
Figure 21: Bighorn sheep CT ROI selection.....	38
Figure 22: MATLAB evaluation validation t-tests.....	40
Figure 23: Velar and trabecular bone property measurement comparisons.. ....	41
Figure 24: Linear regression plots of velar properties by horn curl length. Dashed lines show the 95% confidence bounds of each regression... ..	42

# **Chapter 1: Introduction**

## **1.1 Overview of biomimicry and purpose**

Biological materials science research has been an increasingly promising field of materials study. This is due in part, to the discovery of distinctive and extraordinary biologically generated materials. These materials typically incorporate specific and organized hierarchical and composite structures which yield remarkable mechanical properties[1]. In the past, study into biomimicry has advanced technology in fields of medicine, energy, and transportation. As an example, medical needles have been innovated through the mimicry of mosquito mouths which utilize less force and damage skin less during insertion[2]. The purpose of this study was focused on the identification and characterization of unique examples of porous bone structures as potential subjects for continued biological materials research and biomimicry. Trabecular bone structures examined in this study were sampled from the proximal tibias of grizzly bears, cave bears, and edmontosaurs. The sail-like structure of bighorn sheep horn core bone was also examined based on its unique appearance and function.

## **1.2 Bone Adaptations To Mechanical Loading**

Bone is classified into either cortical or trabecular morphological structures depending on its porosity. The first of these bone structures, cortical bone, is a densely packed material consisting of mineralized hydroxyapatite bound to collagen fibers. This bone structure utilizes a hierarchical structure of fiber oriented layers which come together to form osteons. Cortical bone has a large elastic modulus compared to trabecular bone and other biological tissues which grants it stiffness in bending and compression. Animals use the stiffness and rigidity provided by bones as lever arms by which muscle forces are exerted on the world around them. Bone stiffness also

serves to protect an animal's vital organs from harm by absorbing energy from impacts through elastic and plastic deformation. In this regard, bone is a key structural and protective framework in the body due to its stiffness as a biological material.

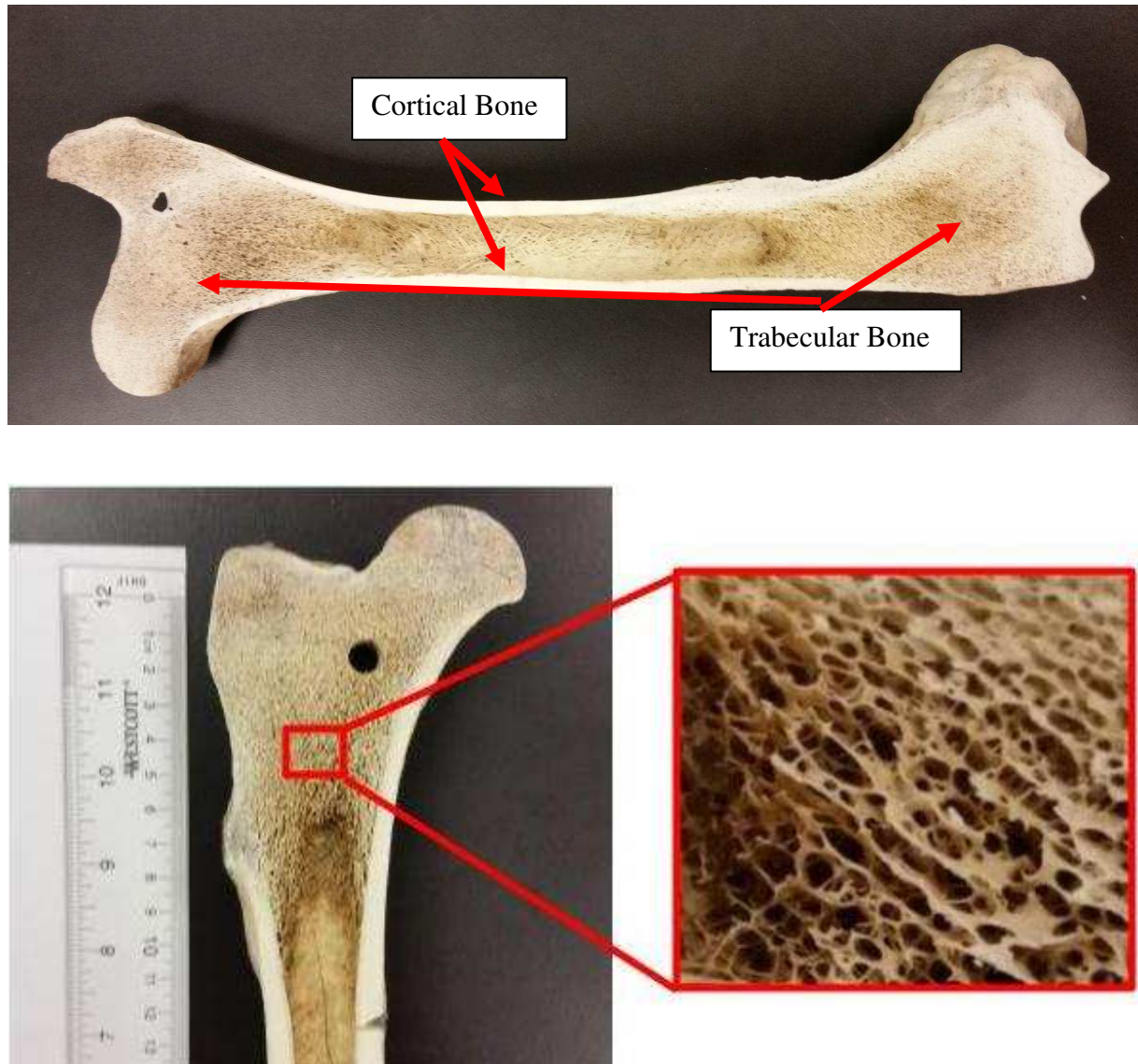


**Figure 1:** Above: cortical and trabecular bone examples and locations in moose femur. Below left: a cutaway of the proximal femur of a black bear. Below right: A zoomed in view of the trabecular bone structure of a black bear femur.

Bone consists of a composite material structure composed of cross-linked organic collagen fibrils bound together with biomineralized inorganic hydroxyapatite crystals[3]. The varied fractional composition of these components, in addition to varied collagen fiber

alignments, results in large variations in bone material properties on a micro scale[4]. These composite matrices are further ordered into morphological structures at the macro scale (i.e., cortical and trabecular bone), which contribute greatly to the overall mechanical properties of the bone. These structures are referred to as cortical bone, and trabecular bone. The cortical and trabecular structures of bone combine in long bones, spinal disks, and skulls to provide additional strength to these bone structures without compromising weight.

Functionally, bone is a uniquely specialized biological material which fulfills two competing goals in an animal's body. First, bone serves to provide structural integrity to the body. The structural aspect of bone is important in both protecting an animal's vital organs as well as providing a mechanism for ambulation through mechanical advantage[5]. Second, bone provides a means to store minerals necessary to everyday functions within the body by embedding these minerals in its extracellular matrix[6]. As a material, bone is composed of both organic type-1 collagen fibrils and inorganic hydroxyapatite mineral crystals. Organic collagen is a protein which provides toughness and strength to bone through its ductility and protein cross linking [7]. Material properties of type-1 collagen have been measured to be  $2.9 \pm 0.1$  GPa [8]. Inorganic hydroxyapatite mineral crystals, composed primarily of calcium and phosphorous ( $\text{Ca}_{10}(\text{PO}_4)_6(\text{OH})_2$ ), are brittle and provide stiffness to bone [9]. Hydroxyapatite has a measured modulus of elasticity of 114 GPa [10]. These components of bone come together to form a hierarchical structure with mechanical properties which blend the properties of both organic collagen and inorganic hydroxyapatite.

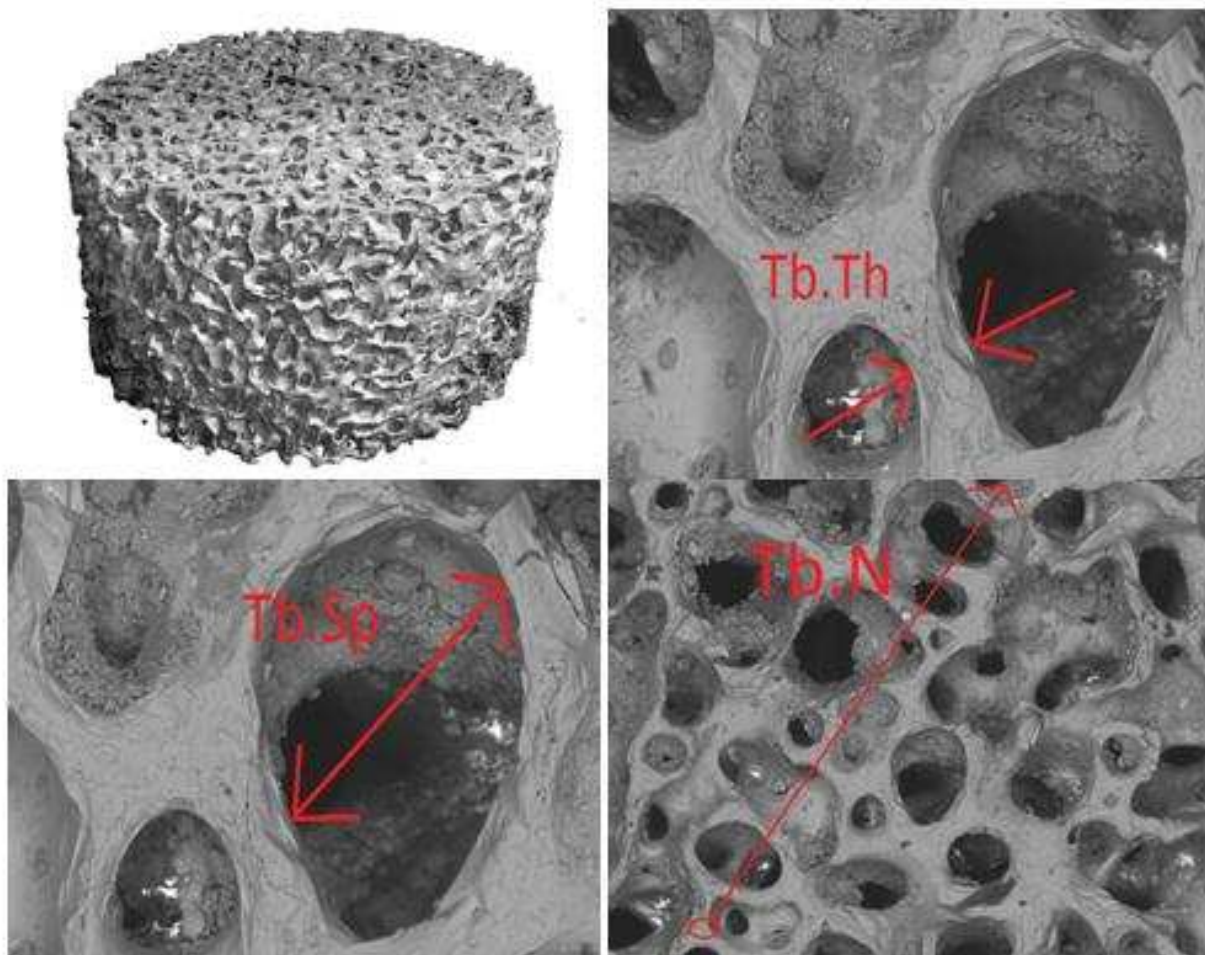


**Figure 2: Trabecular bone morphological property diagrams. Upper left: Bone volume fraction given by total bone volume relative to total volume. Upper right: Thrabecular thickness shown as the thickness of the bone formation. Lower left: Trabecular separation shown as the distance between bone formations. Lower right: Trabecular number shown as the count of bone formations over a distance.**

Bone mechanical properties depend on many factors. On a microstructural level, bone mechanical properties differ depending on: fractional mineralization, collagen fiber alignment, collagen cross-linking, strain rate and hydration[4,11-15]. In a single bone, the geometry, anisotropy, porosity, and morphology all contribute to the mechanical response during loading [16-19]. Trabecular bone morphology is expressed as the quantification of several different physical attributes including measurements of total fractional porosity, strut frequency, thickness, separation, and connectivity[20]. These structural and material properties are primarily determined from genetic code during primary bone formation. However, bone remodeling

further adapts bone microstructure to more optimally fulfill its purpose through a process called mechanotransduction [21]. In addition to fine tuning a bone's structure to its mechanical environment, bone remodeling repairs and maintains bone by removing microdamage from fatigue or extreme loading [22-24]. The combination of primary bone formation and secondary bone remodeling contributes to the variability in measured bone properties.

In humans, hip joint forces acting on bones have been measured at approximately 280% total body weight during walking and 480% total body weight during jogging [25]. These routinely large forces, associated with basic ambulation highlight the importance of the strength and stiffness of bones as a structure. Bone has evolved as a biological material to be capable of withstanding routinely large forces and avoid catastrophic damage during regular activity. As a structural system, bone exhibits remarkable mechanical material properties which are stronger than some steel alloys when normalized by density. [26-28] Overall, weight is important to an animal's skeletal structure because their bones must be light enough that providing the necessary structural integrity is not too metabolically costly to the animal[29].

Bone provides the main reservoirs for calcium, phosphorus, and magnesium in the body [30]. By storing these necessary minerals in bone, mineral concentration in the blood can be regulated from mineral storage in addition to daily diet. However, bone's role as a mineral storage center conflicts with bone's role as a structure. In this case, having larger mineral stores means that the bones themselves must be larger. This scenario results in having bones which are both unnecessarily large for the magnitudes of the stresses exhibited on them and too heavy for metabolic efficiency in the animal. In order to balance these conflicting roles, bone goes through an optimization process of formation and resorption[31]. This process maintains the blood

mineral levels necessary for the body to function while making sure that the bones are sturdy enough to withstand the stress of daily usage.

The role of bone formation and resorption in the optimization of bone architecture was first proposed in 1892 by Julius Wolff[32]. Wolff's proposal suggested that changes in the function of a bone corresponded to changes in the internal structure of the bone according to mathematical laws[33]. Furthermore, Wolff's law is understood to represent bone formation and resorption as a process where bone is deposited at locations of high stress and resorped at locations where stress is low[34]. Bone optimization is not governed strictly by mathematical laws, however, Wolff's Law is generally accepted as the concept that bone structure is influenced by its habitual mechanical environment. The influence of the mechanical environment of bone on the bone structure is seen in the regulation of bone formation and resorption during the functional use and disuse of bone[35]. Wolff's law is often combined with the process of mechanotransduction to explain the living nature of bone and how it is self adjusting towards an optimized support structure in the body.

Mechanotransduction is regarded as the process by which mechanical stimuli is converted into biochemical activity[36,37]. In bone, the activation of osteo-regulatory osteoblasts, bone forming cells, and osteoclasts, bone resorping cells, is triggered as a result of strain sensitive osteocytes through biochemical pathways[38]. Studies have shown that bone on a continuum level has a regulated peak strain between 2000-3000 microstrain. This microstrain value is common between several species and is believed to be a targeted value of strain in bone which regulates a 2-3 factor margin of safety between functional strain and yield strain of bone in an animal[39]. In order to achieve these levels of dynamic strain similarity, osteoblasts and osteoclasts perform bone remodeling to alter the bone's morphology. In altering the shape of the

bone, the osteo-regulatory cells optimize the structure of a bone to reduce maximal dynamic strain. This optimization process enables bone to better fulfill its function and reduce the likelihood of fracture while minimizing weight.

The combined concepts of Wolff's law and mechanotransduction leading to bone remodeling is true not only for compact cortical bone, but also in the porous trabecular bone. Similar to the concept of dynamic strain similarity discussed previously, trabecular bone was found to alter its structure in order to maintain uniform, isotropic peak strains[40]. Expanding on the theories given by Wolff's law for bone structure optimization, several studies have generated computerized models simulating bone resorption and formation in response to externally applied strain [41,42]. In one of these models, bone morphology optimization minimizing strain energy resulted in increased Tb.Th and decreased Tb.Sp in compressive regions after morphological optimization. The numerical results of the optimization agreed well with measured trabecular bone architecture. The agreement between simulation and experimental results suggests that optimization of strain energy through targeted bone remodeling influences the topology of bone struts in regions of high strain. Another computer model tested compressive and tensile loading simulations to optimize trabecular morphology by minimizing strain energy in a proximal femur. The resultant computer optimized morphology was determined to have strong resemblance to clinically measured trabecular morphology[43]. In vivo examples of bone optimization and Wolff's law can be found in studies involving extended disuse or unloading of a bone such as animals in long-term spaceflight. Strain optimization in these disuse mechanical environments resulted in net resorption of mineralized bone tissue in trabecular and cortical bone due to the decrease in applied bone stress[44]. By studying and understanding the structure-function

relationship of trabecular bone in animals, better attempts at targeted bioinspired material design can be identified and pursued.

### **1.3 Overview of Trabecular Bone**

Trabecular bone is a highly porous bone structure analogous to a cellular solid in porosity, morphology, and energy absorptive properties [45]. When cellular solids such as structural foams or trabecular bone are loaded in bending, they are typically characterized by a three-phase progression stress-strain response. First, as strain increases, there's a brief region of elastic deformation characterized by the elastic modulus of the cellular solid. This elastic region is followed by a second region of plastic crushing or buckling of the cell struts. Finally, there is a region of cell densification where buckled struts or cell walls compress and bulk failure ultimately occurs[46]. Cellular solids which exhibit this loading process have smaller observed values for elastic modulus, due to porosity, and larger observed values for strain energy density, due to the region of plastic collapse. These observed differences are compared to what is typically observed in the mechanical response of a solid composed of the same material.

Continuum material properties for foam-like structures, such as trabecular bone, are dependent on three primary factors: the material of the struts, the shape and topology of the foam cells, and the relative density of the foam [47]. However, due to osteocyte-driven bone remodeling, in vivo trabecular bone has greater strain energy density than engineered foams over the life of the cellular solid. This is because bone remodeling extends the lifelong ability of trabecular bone to handle functional loads by repairing cracks caused by fatigue or extreme loading [48]. In addition to bone remodeling, mechanotransduction within trabecular bone leads to the reinforcing of high stress bearing struts. This reduces potential failures of weak struts

further mitigating possibility of catastrophic failure and extends the mechanical viability of trabecular bone.

Due to the nature of trabecular bone as a cellular solid, the mechanical response of trabecular bone is highly dependent upon its morphological structure[49-53]. By definition, morphology is the study of the form or function of an organism or any of its parts [54]. As stated previously, trabecular bone morphology is expressed as the quantification of several different physical attributes including measurements of total fractional porosity, strut frequency, thickness, separation, and connectivity[20]. These measurements are written as bone volume fraction (BV/TV), trabecular number (Tb.N), trabecular thickness (Tb.Th), trabecular separation (Tb.Sp), and connectivity density (Conn.D) respectively (fig 2). BV/TV is given as the total volume of bone relative to the total volume of measurement. Tb.Th is measured as the mean diameter of the bone struts. Tb.Sp is measured as a mean of the maximal diameters of spheres fit between bone formations. Tb.N is a count of bone formations over a distance. Using these measurements, scientists have attempted to relate measured trabecular bone parameters to various mechanical stimuli. Specifically, trabecular bone morphological measurements for Tb.Th, Tb.Sp, and Tb.N have been shown to scale relative to total body mass of an animal[55]. In the same study, BV/TV had no significant scaling relationship with body mass. Additional scaling relationships in trabecular bone have been explored based on age and osteo-regulatory diseases with varying degrees of success[56,57].

As mentioned previously, trabecular bone mechanical properties are dependent upon the morphological structure due to its classification as a cellular solid. Research into trabecular bone mechanical properties has indicated that BV/TV correlates strongly with elastic modulus[58]. Values for Tb.Th, Tb.Sp, and Tb.N are more closely correlated to BV/TV than to overall elastic

modulus. This is expected because the Tb.Th, Tb.Sp, and Tb.N measurements are descriptors of how the bone mass is represented and distributed in the trabecular volume. Because of this, trabecular bone properties of Tb.Th, Tb.Sp, and Tb.N, are more likely to exhibit changes in trabecular bone moment of inertia than on elastic modulus. Both elastic modulus and material moment of inertia are important characteristics in determining how an object will respond to a compound loading environment involving axial and bending loads. By investigating the trabecular bone properties, scientists can gain increased understanding into how trabecular bone functionally responds to mechanical stimulation. This understanding can further be applied towards potential bioinspired material design taking advantage of the biological optimization of trabecular bone.

Many animals utilize bone to fulfill unique and incredible functional roles. As a result of this, bones have been shown to possess vastly differing material properties in accordance with better serving their functional goals. In example of this, is a study on the mineral properties of bones used in 3 unique biological applications. The bones studied included deer antlers used in impact loads, cow femurs used for structural support, and whale bullas used for acoustic sensitivity[59]. In this study each bone type was measured for its tensile strength, work of fracture, and density. Deer antler was shown to have a remarkably high work of fracture with a relatively low fractional mineral content. High work of fracture in antler means that the antler is highly energy absorbent and resistant to failure in impact loading. Failure resistance lends to the functionality of deer antlers by dissipating energy and protecting antlers through the duration of the mating season. The cow femurs tested had exceptional bending strength with an average fractional mineral content. This is beneficial to cows due to the bending dominated usage of long bones in terrestrial animals. Finally, the whale bulla was measured to be exceptionally dense and

extremely brittle with a relatively high fractional mineral content. The high density of the whale bulla increases the acoustic impedance of the bone making it more sensitive to sound waves. The high density along with the physiological connection of the bulla allows the whale to hear exceptionally well underwater making it easier to find mates. In each of these examples, the bone has evolutionarily adapted fractional mineral content to better fulfill their unique functional purposes. In a similar fashion, the structure of trabecular bone has potential for adapting morphologically to better fit unique mechanical environments such as those seen by bone in the long bones of grizzly bears, cave bears, edmontosaurs, and bighorn sheep horn cores. By studying the bony structures relevant to high force or high strain rate impact loading, the adapted qualities of trabecular bone structures can be applied towards future work in bioinspired structural foam designs.

#### **1.4 Grizzly Bears and Cave Bears**

Trabecular bone in grizzly bears (*Ursus arctos horribilis*) showcases a unique functional case of trabecular bone in extant mammals. Long periods of disuse or inactivity in animals has typically been shown to increase bone resorption[28]. However, grizzly bears, which routinely experience long periods of disuse during the hibernation cycle, have been shown to suppress bone loss in their trabecular bone during these periods of disuse [60]. As a result of this unique property, the morphological trabecular bone properties in grizzly bears have already been well explored. However, the trabecular bone morphological properties of the cave bear (*Ursus spelaeus*), a near relative of the grizzly bear through the common ancestor *Ursus etruscus*, have not been well explored[61].

Cave bears went extinct an estimated 24,000 years before present from potential environmental factors and left behind evidence of their existence in the form of fossilized

bones[62]. Bone is unique from other biological materials because bone can, in part, resist decomposition through fossilization. As discussed previously, bone is a composite biological material which is made up of both organic collagen tissue and mineralized crystalline hydroxyapatite. After an animal's death, it is possible for the body to become fossilized thus preserving parts of the body. The process of fossilization follows the dissolution of organic tissue and re-crystallization of mineralized tissue as the surrounding sediment undergoes the process of diagenesis. Resulting fossilized tissue preservation is dependent upon time, temperature, and environmental pH during fossilization[63]. The unique aspect of the mineralized structure of bone in the body allows for researchers in the present to study extinct species that lived long before our present age.

From the fossils identified as cave bears, scientists have suggested that male cave bears had an average body mass between 354-634 kg depending on prediction technique[64]. Modern grizzly bears have been measured to have an average male body mass of 192 kg[65]. Based on the body mass measurements and estimations, cave bears are expected to be larger than their modern relatives. It is unclear whether cave bear trabecular bone behaved similarly to grizzly bear trabecular bone in disuse situations. However, study into the morphological properties of cave bear trabecular bone may give insight into the functional adaptation of trabecular bone in a larger species from prehistoric times.

#### **1.4.1 Grizzly Bear and Cave Bear Hypothesis**

Cave bears have the same bone volume fraction, greater trabecular thickness and separation, and lower trabecular number than grizzlies bears because cave bears were more massive.

## 1.5 Edmontosaurus

Unlike extant animal species, many dinosaurs were capable of growing to gigantic sizes with some weighing upwards of 70,000 kg as estimated from fossil records[66]. Gigantism, and the massive forces applied to bones of animals of gigantic body masses, showcases a unique functional usage of trabecular bone which has yet to be explored by modern science. Fossilized dinosaur bones date back tens of millions to hundreds of millions of years and physically represent many of the largest animals to have ever walked the face of the Earth. Finding fossilized dinosaur bones is an extremely rare circumstance which lends to a reluctance and absence of research in dinosaur trabecular bone. However, among the dinosaur fossils currently discovered, excavated and in collections, the edmontosaurus is one of the most common. This makes the edmontosaurus a great candidate for trabecular bone studies relative to gigantism.

The edmontosaurus is a genus of dinosaur which stems from the Hadrosauridae family (duck-billed dinosaurs). The typical adult edmontosaurus is expected to have weighed around  $7936 \pm 1991$  kg [67]. Recall that bones under load during ambulation can experience forces equivalent to several times the total body mass of an animal. In dinosaurs this principle can result in massive forces being applied to the bone [68-70]. Through Wolff's law, the form of a bone adapts to optimally fulfill the mechanical function that it serves. Therefore, the trabecular bone within the long bones of edmontosaurus could theoretically be highly adapted in its morphology for withstanding large forces. Quantifying the underlying trabecular bone properties using micro computed tomography ( $\mu$ CT) could explain how biological structures were able to support the mechanical loadings of such massive animals [68]. Additionally, comparing the trabecular bone scaling relationships of dinosaurs to extant species could explain why animals today cannot achieve the same levels of gigantism found in dinosaurs.

### 1.5.1 Edmontosaurus Hypothesis

Edmontosaur trabecular bone will exhibit morphology utilizing comparable BV/TV, high Tb.Th and Tb.Sp, and low Tb.N as compared to extant animals because Tb.Th, Tb.Sp, and Tb.N scale with body mass and edmontosaur body mass was larger than extant mammals.

### 1.6 Bighorn Sheep



**Figure 3: Bighorn sheep skull with horn cutaway.**

Recent biological materials research has begun investigation into various horn structures and the reasons behind their exceptional toughness, durability and energy absorptive properties [71-74]. In particular, bighorn sheep (*Ovis canadensis*) have a unique and highly adapted horn structure to absorb energy from repeated impacts during mating rituals. It is estimated that these impacts can carry forces up to 3,400 N, yet impact does not seem to cause significant lasting brain damage [75]. The horns of bighorn sheep are never shed throughout the life of the animal

and are composed of both a highly durable keratin sheath and an osseous horn core. The keratin sheath has been noted to be an extremely tough material, having a high work to failure ratio, and insensitivity to notching [76]. Underneath the keratin sheath, the horn core extends from the skull approximately one third of the total length of the horn. The horn core is composed of a hard cortical bone shell that encompasses a volume of porous bone.



**Figure 4: Left a cutaway of a bighorn sheep horn core revealing the sail-like bone formations within. Right: a cutaway of traditionally regarded trabecular bone from a black bear femur.**

The porous bone found in bighorn sheep horn core is unique in appearance and function in comparison to what is considered trabecular bone (fig 4). The bone inside the bighorn horn core appears to have more sail-like bone than the rod-like bone found in trabecular bone. These thin membranes of bone within the bighorn sheep horn core bear a resemblance to the sails of a sailboat, therefore the bone that fills the horn core will be referred to as “velar bone” (vela meaning sail in latin) rather than trabecular bone. The velar bone in bighorn sheep horn core is unlike common long bone trabecular bone in several ways. Long bone trabecular bone has rod-

like struts approximately 100 to 200 microns in thickness, whereas the bighorn velar bone has more sail-like struts, approximately 2 to 5 mm in thickness. These features and additional porous bone morphological measurements have not yet been quantified in measurements common to trabecular bone (ie. Tb.Th, Tb.N, and Tb.Sp).

These morphological properties of velar horn core bone are of great interest from a functional perspective. Most research into bighorn sheep horn mechanical material properties has been focused on the horn keratin, with little focus being placed on the mechanical role of the horn core itself[71-74,76]. In recent research, it was noted that the velar bone within the horn core accounted for a surprising 442% reduction in brain cavity rotational acceleration and was responsible for absorbing the most strain energy during impact, despite the high work to failure of the keratin sheath [77]. This finding suggests that there is a uniquely evolved adaptation in bighorn horn core velar bone that is lending to the horn's ability to absorb high impact energy. The characterization of measured structural properties within the velar bone in bighorn sheep also has a high potential for inspiring the design of high impact resistant and energy absorbent foams.

### **1.6.1 Bighorn Sheep Hypothesis**

Bighorn sheep horn core bone fulfills the role of withstanding repeated high impact loading during mating rituals as opposed to the low impact, bending dominated role of long bones. Therefore, bighorn sheep horn core velar bone properties for bone volume fraction, velar thickness (V.Th), velar separation (V.Sp), and velar number (V.N), will be significantly different compared to trabecular bone properties in long bones.

## **Chapter 2: Methods and Results**

### **2.1 Grizzly Bear and Cave Bear Methods and Results**

#### **2.1.1 Sample Information**

This study used 4 grizzly bear tibia bone archived samples, ages 1 to 4, (2 male and 2 female) previously harvested from humanely sacrificed animals at Washington State University. The bones were stored frozen at -20 degrees Celsius prior to testing. Four cave bear tibia fossils (sex unknown) were collected and provided for use by Dr. Grandal-d'Anglade of the University A Coruña.

#### **2.1.2 Sample Preparation Procedures**

Each tibia sample was prepared for trabecular bone morphology measurements by removing a trabecular bone core sample from the tibial plateau. Trabecular bone core samples were drilled from the medial portion of the lateral condyle using a 0.5 inch outer diameter diamond sintered core drill bit. The drilling setup included a drill press, core drill spindle, water pump, and a table vice (fig 5). During drilling, water was pumped through the center of the coring drill bit to cool the sample and flush debris from the drill. The drill bit was plunged into the sample a depth of 1.5 inches from the tibial plateau surface. Tibial cores were removed from the grizzly bears by cutting in from the side approximately 1.2-1.5 inches from the tibial plateau using a desktop band saw. The cave bear trabecular bone cores were removed from the tibia by inserting a scoopula into the drill hole and applying a sideways pressure until the core sheared from the sample bone.

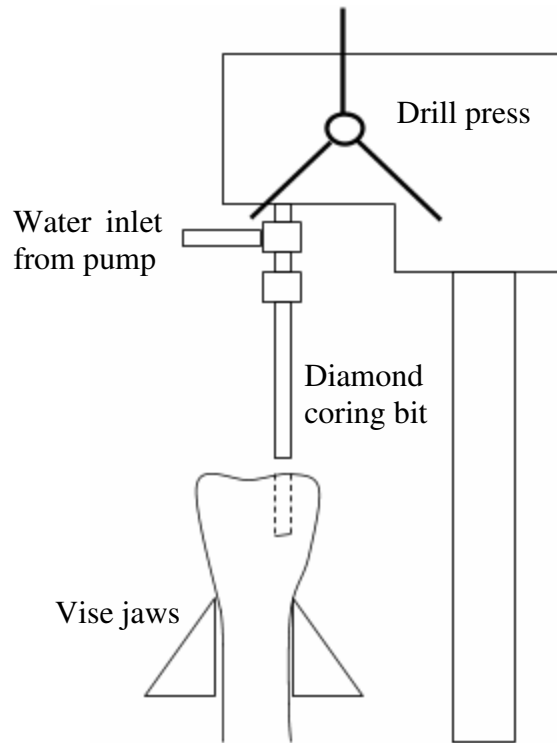


**Figure 5: Diagram depicting the coring setup**

### **2.1.3 Sample Measurements**

The tibias for the cave bear and grizzly bear were each measured for their total length, midshaft diameter, and tibial plateau medial lateral and A-P width. These length measurements were taken using a pair of digital calipers as shown in figure 6.

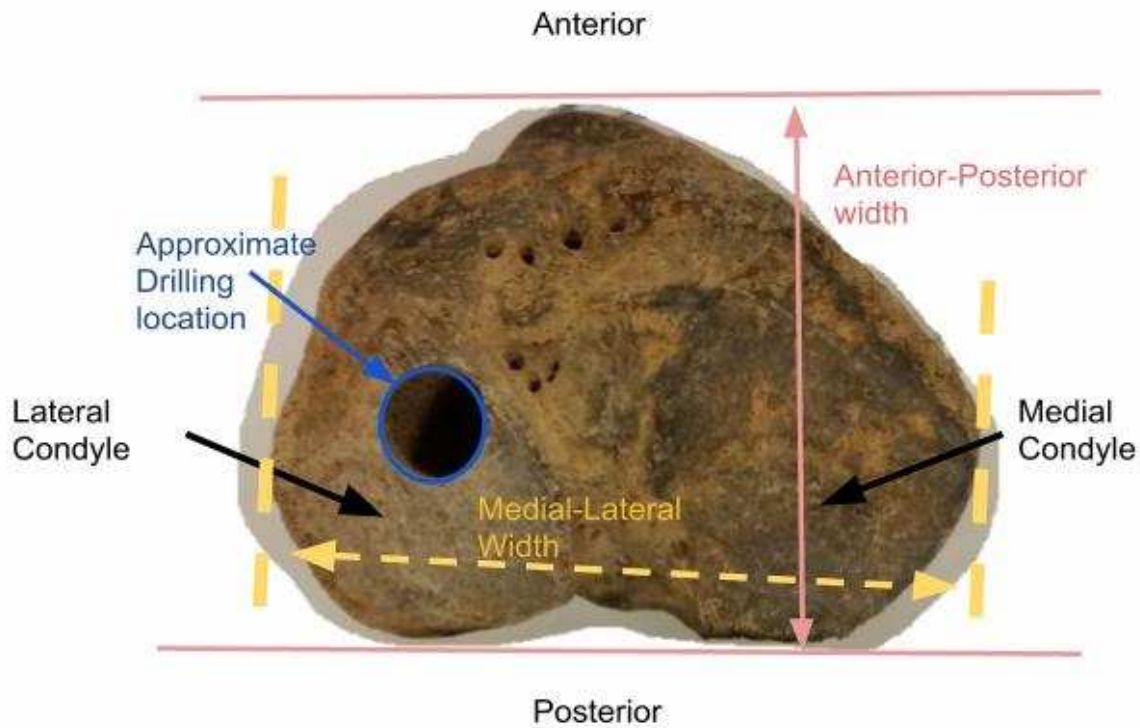


**Figure 6: A depiction of a cave bear tibial plateau with markings indicating how the width measurements were made for the tibial plateau in red and yellow. An example of the drilling location is highlighted in blue.**

The trabecular cores for the cave bear and grizzly bear samples were imaged using a SCANCO micro computed tomography ( $\mu$ CT) (SCANCO  $\mu$ CT 80 Medical, Switzerland) machine. Each sample was imaged at high resolution with 8W bulb power at 70 kVp excitation voltage. Cave bear samples were scanned inside of a copper foil tube. The copper foil tube serves as a filter to scatter low frequency X-Ray radiation and prevent image artifacts due to beam hardening. This prevents distortion in the image of high density objects in radiographic imaging [78]. The sample region of interest was selected to be a 5 mm height at a distance of 1-2 mm distal to the physal scar or physis. This distance was chosen in order to exclude potential unmineralized bone from the volume of interest. The resulting scan was contoured before evaluation to exclude the outer 0.1-0.2 mm (approximately 1 - 2 trabecular thicknesses) of the trabecular bone core. The exclusion of this material was performed to exclude potentially

damaged bone from the evaluation region. The trabecular bone morphology measurements were performed using SCANCO's trabecular bone evaluation software.

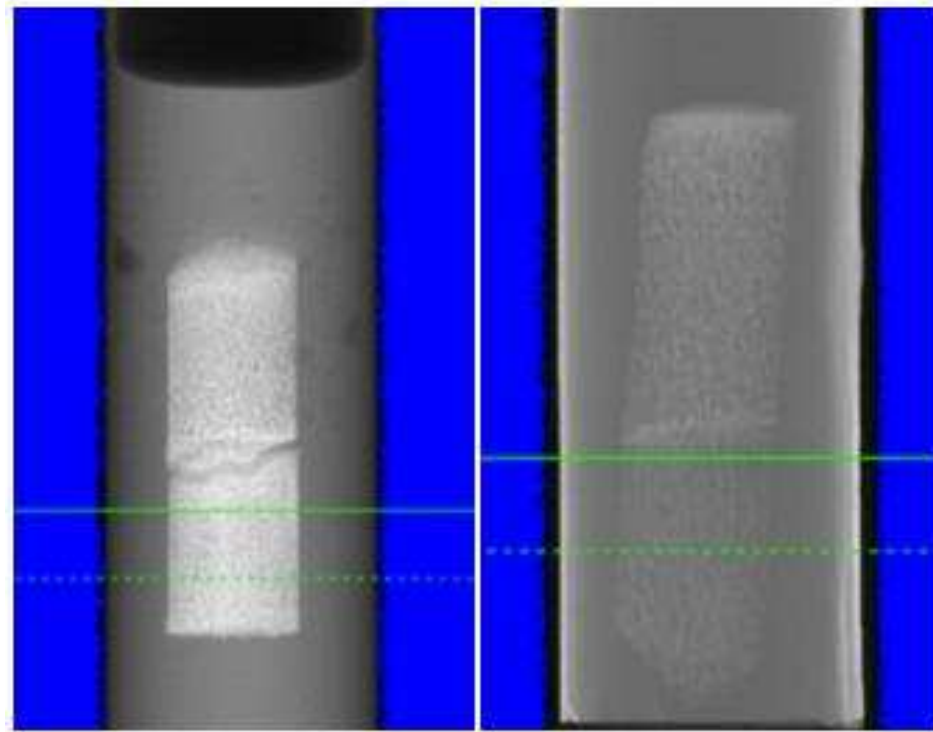


**Figure 7: Left: grizzly bear  $\mu$ CT scout view detailing evaluation region distal to the physis. Right: cave bear  $\mu$ CT scout view showing evaluation region distal to the physeal scar.**

#### **2.1.4 Cave Bear and Grizzly Bear Statistics**

Cave bear and grizzly bear results for size measurements and trabecular properties were compared using paired-sample t-tests with a 95% confidence level.

### 2.1.5 Grizzly Bear and Cave Bear Trabecular Bone Morphology Results

The total length measurements between the cave bears and grizzly bears were not significant (fig. 8) ( $p = 0.0591$ ). However, the measurements for midshaft diameter and plateau width, for both the medial lateral and anterior posterior directions, were all significantly different. The cave bear tibias measured larger than the grizzly bear tibias as seen in figure 9.

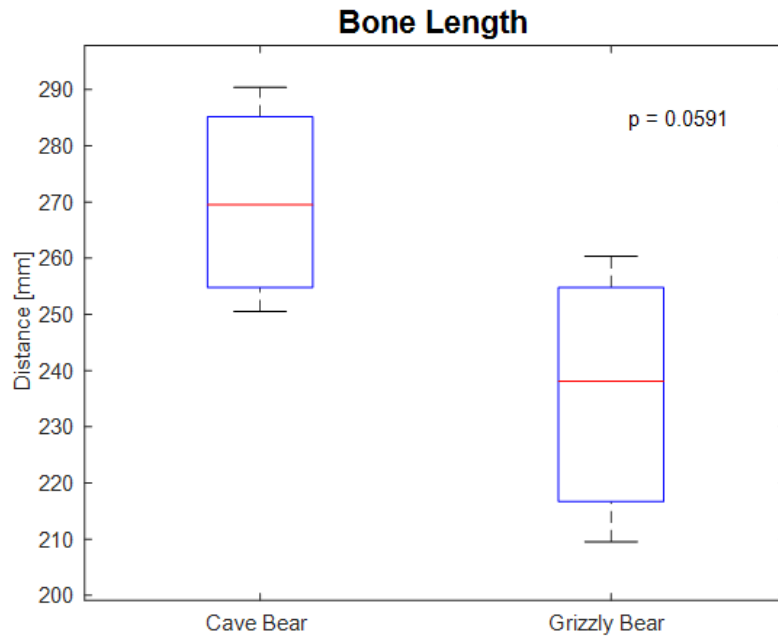
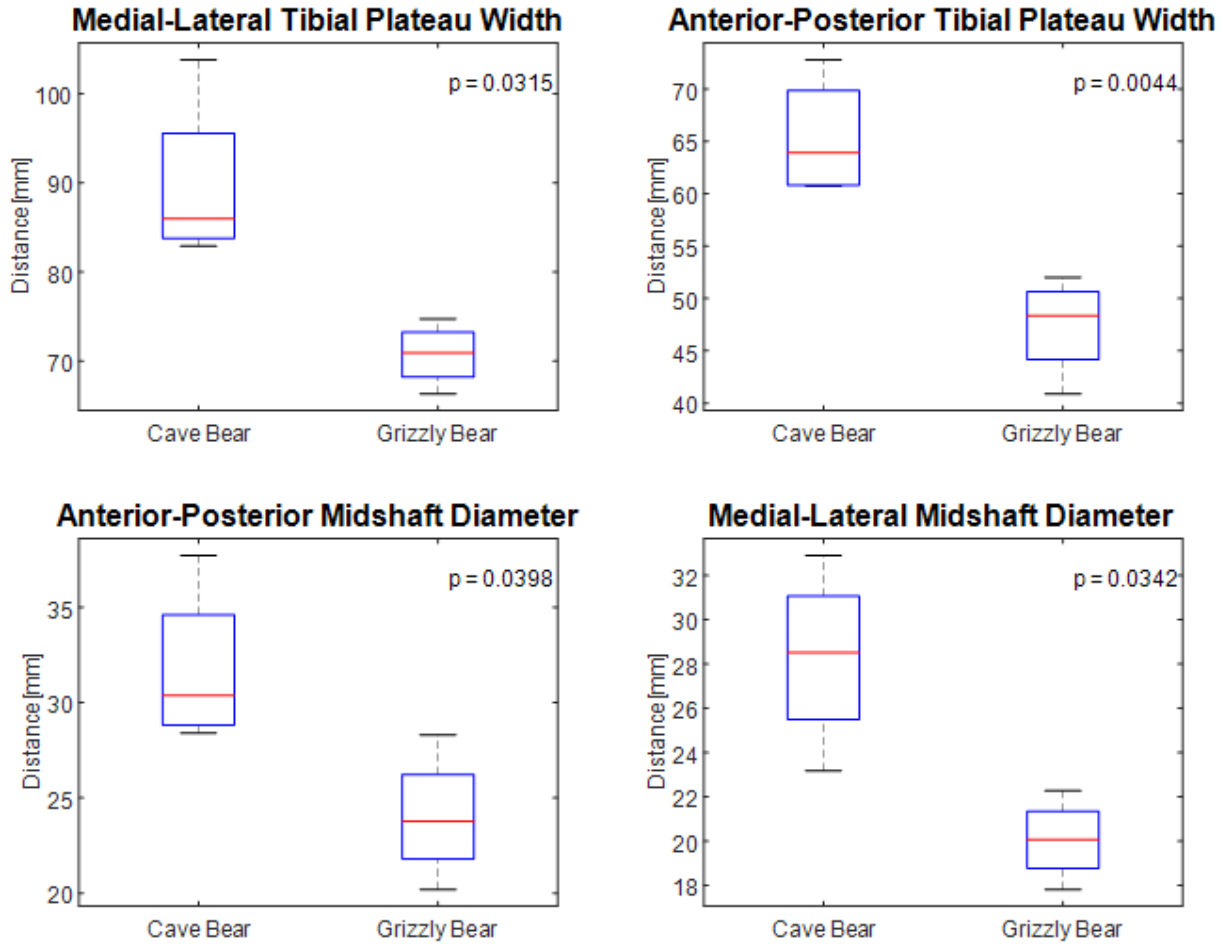
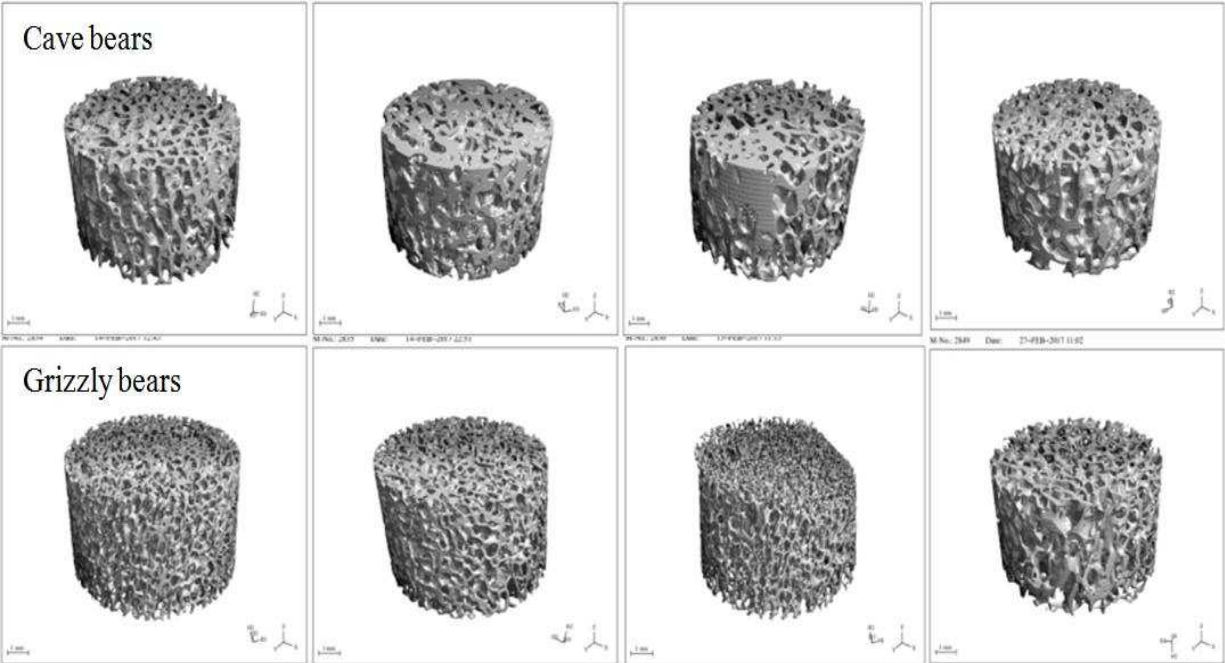


Figure 8: Measured bone lengths compared between cave bears and grizzly bears.



**Figure 9: Plateau width and midshaft diameter measurement t-tests.**

The  $\mu$ CT trabecular bone morphology results (fig 11) showed that the BV/TV was larger in cave bears than in grizzly bears ( $p = 0.0094$ ). Cave bear trabeculae were on average 80  $\mu$ m thicker than grizzly bear trabeculae ( $p = 0.0183$ ). Tb.N was not significantly different between cave bear trabecular bone and grizzly bear trabecular bone ( $P = 0.9946$ ). Lastly, cave bear Tb.Sp was not significant from the measured grizzly bear Tb.Sp ( $P = 0.2694$ ).



**Figure 10: Top row: 3 dimensional reconstructions of cave bear  $\mu$ CT scan volumes. Bottom row: 3 dimensional reconstructions of grizzly bear  $\mu$ CT scan volumes**

From 3D reconstructions of the  $\mu$ CT scans, the results seen in the trabecular morphological measurements can be visualized. In particular the larger bone strut thickness of the cave bear trabecular bone is easily noticeable as seen in figure 10.

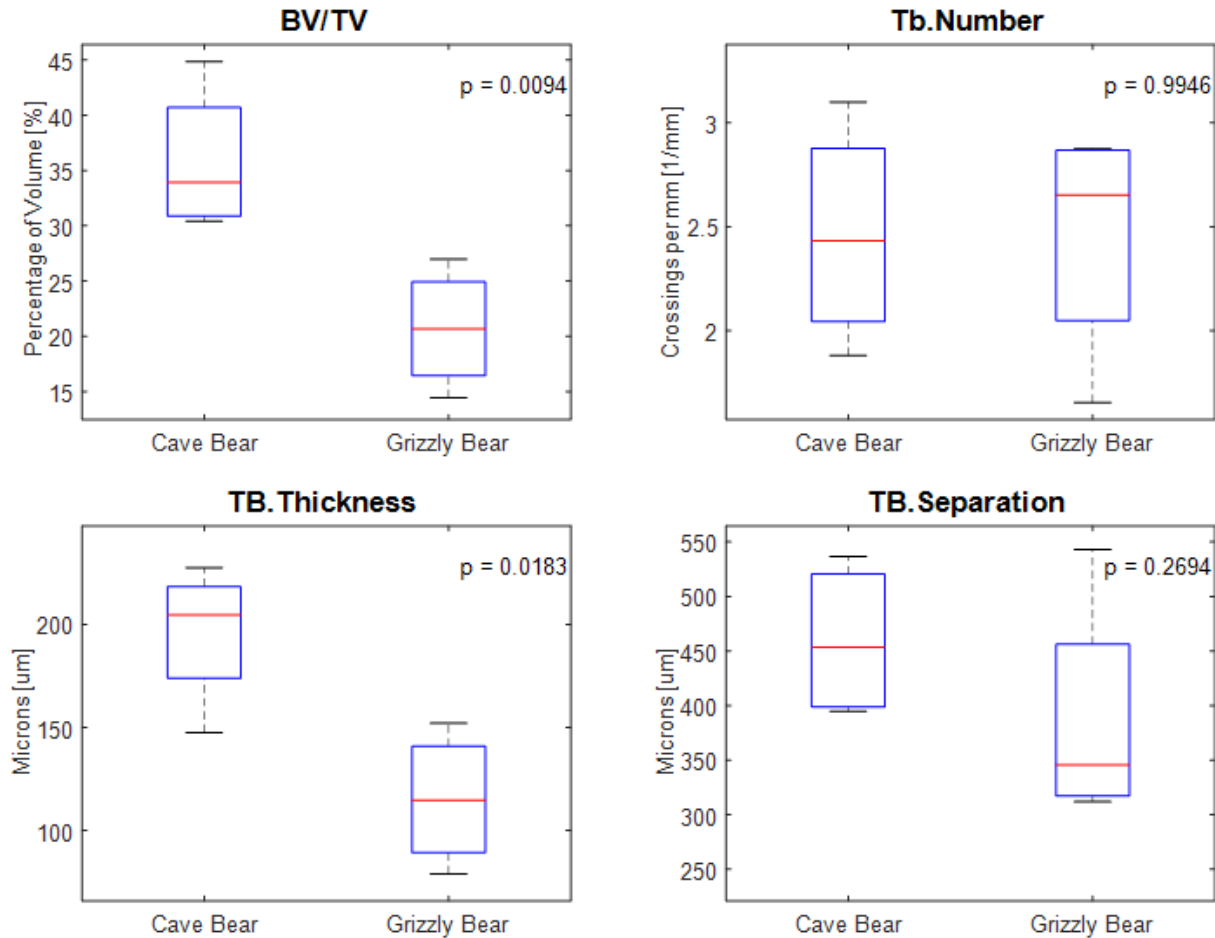


Figure 11: Trabecular bone morphological property comparisons between cave bears and grizzly bears.

## 2.2 Edmontosaur Methods and Results

### 2.2.1 Edmontosaur Samples

This research used 7 *Edmontosaurus annectens* tibia bone samples of unknown sex and age. These samples were provided for this research by Dr. Fiorillo of the Perot Museum of Nature and Science. The bones were identified to have belonged to juveniles through inspection of size. The fossils from the Perot Museum of Nature and Science were broken off at varying points along their diaphyses and were collected from a single dig site in the state of Alaska. An additional 4 *Edmontosaurus regalis* tibia fossils (sex and age unknown) were provided for use in this research by Dr. Sertich of the Denver Museum of Nature and Science. These fossils were

collected from dig sites in the Hell Creek formation dating back to the Maastrichtian age. The 4 bones used in this research were identified as belonging to adult edmontosaurs based on size.

### **2.2.2 Edmontosaur Sample Drilling Locations**

The drilling of trabecular bone cores from fossils dating back millions of years is a novel process. Due to the effects of fossilization and sedimentation, it was initially unclear whether the trabecular bone in these fossils would be preserved and distinct enough for measurement in a  $\mu$ CT. To scout the possibility of collecting usable core samples for trabecular bone morphology measurements, the juvenile tibia fossils were first scanned in a Gemini Time-of-Flight Big Bore PET/16 slice CT (PET/CT) (Philips Healthcare, Andover, MA). Using the imaging results from these scans, regions of high and low density material could be distinguished (fig 12). Regions of high density were assumed to be regions of high sedimentation with decreased chances of housing measurable trabecular bone. A drill site targeting the lower density material was determined for each juvenile tibia sample. By scouting the bones in a standard PET/CT, 7 out of 7 samples yielded measureable cores without heavy sedimentation.

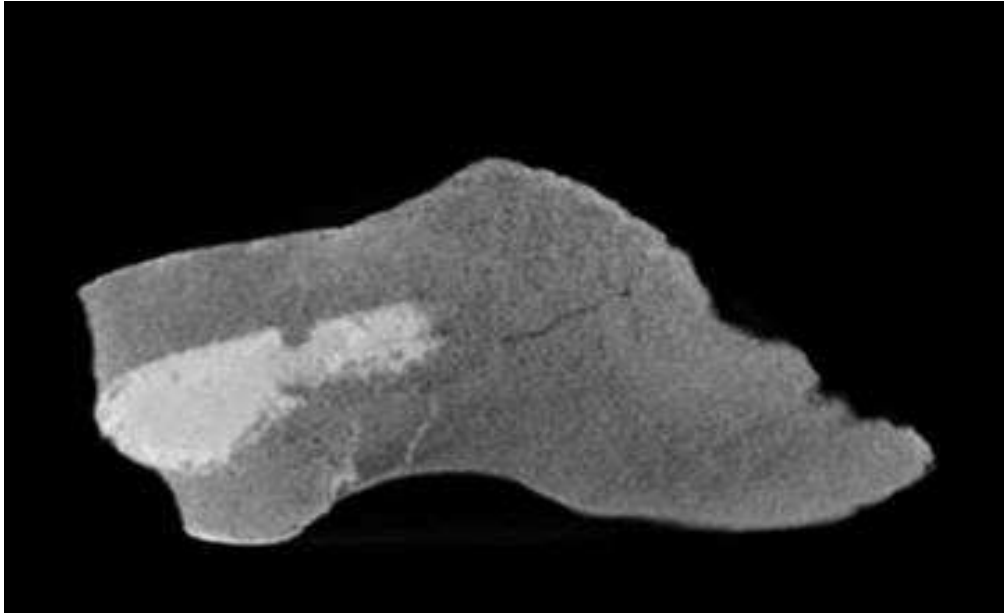


**Figure 12: PET/CT radiograph scout for high and low density regions in fossils.**

Due to the size of the adult edmontosaur samples, there were restrictions to scouting drill locations using a standard PET/CT. Drill locations for the adult samples were all taken from the medial portion of the lateral condyle. Using this method, only 4 measurable core samples could be collected from a total of 6 available bones.

### **2.2.3 Edmontosaur Sample Preparation**

The procedure for drilling the edmontosaur fossils followed methods used in the cave bear grizzly bear research. Each tibia sample was prepared for trabecular bone morphology measurements by removing a trabecular bone core sample from the tibial plateau. Trabecular bone core samples were drilled from the locations determined previously using a 0.5 inch outer diameter diamond sintered core drill bit. The drilling setup for the juvenile edmontosaurs included a drill press, core drill spindle, water pump, and a table vice (fig 5). Due to size restrictions with the adult edmontosaurs, the drilling setup was altered to use a handheld cordless drill instead of an upright drill press. During drilling, water was pumped through the center of the coring drill bit to cool the sample and flush debris from the drill. The drill bit was plunged into

the sample a total depth of 2-3 inches from the tibial plateau surface. Core samples that did not fracture during the drilling process were from the tibia by inserting a scoopula into the drill hole and applying a sideways pressure until the core sheared off.

#### 2.2.4 Edmontosaur Sample Imaging

The trabecular cores for the edmontosaurus samples were imaged using the SCANCO  $\mu$ CT 80 machine. Each sample was imaged at high resolution with 8W bulb power at 70 kVp excitation voltage. Fossil cores were imaged inside of a copper foil filter fit to the inside dimensions of the scanning gantry[78]. The sample region of interest was selected to be a 5 mm height distal to the apparent midpoint of the core sample (fig 13).

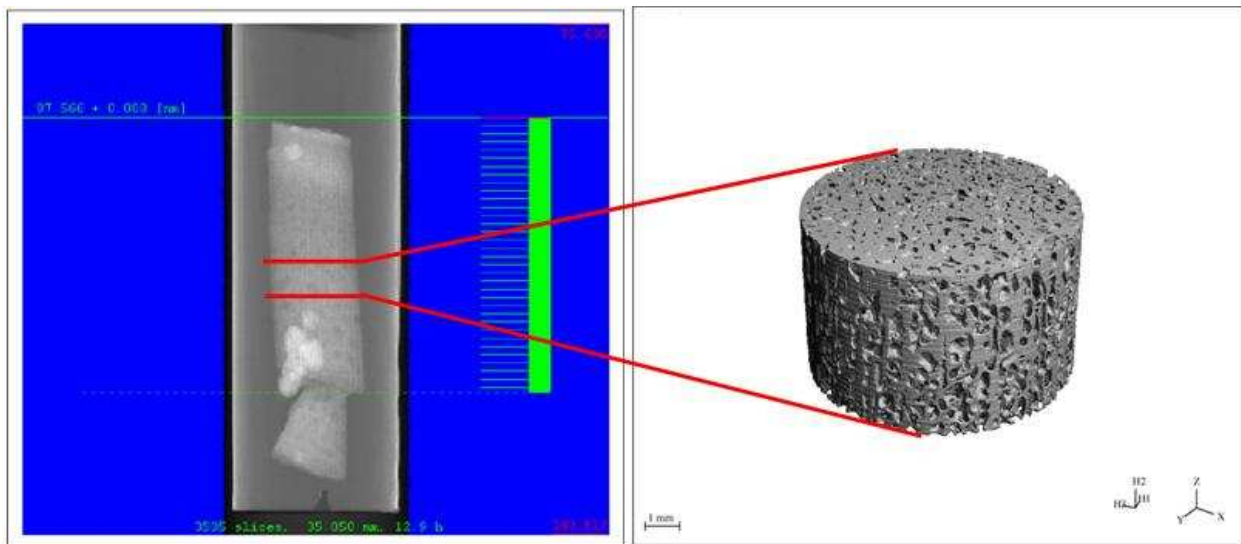


Figure 13: Scout view of edmontosaur core and resulting 3D reconstruction.

This region was chosen because there were no visible landmarks within the fossils, such as a physis, to determine a normalized relative location. The scan began distal to the midpoint in order to exclude bone near to the cortical shell from the volume of interest. The resulting scan was contoured before evaluation to exclude the outer 0.1-0.2 mm of the trabecular bone core (approximately 1 - 2 trabecular thicknesses). The exclusion of this material was performed to

remove potentially damaged bone from the evaluation region. The trabecular bone morphology measurements were performed using the SCANCO software.

### 2.2.5 Edmontosaur Statistics

The resulting trabecular bone morphology measurements were compared against published trabecular bone measurements in tibias for several species of mammals[55]. The results of the edmontosaurs were also compared against the results gathered in the cave bear and grizzly bear research. Edmontosaur measurements were analyzed using a one-way ANOVA with a 95% confidence level for each measurement property. A Tukey-Kramer post-hoc test was performed on the results to determine significance between species groups.

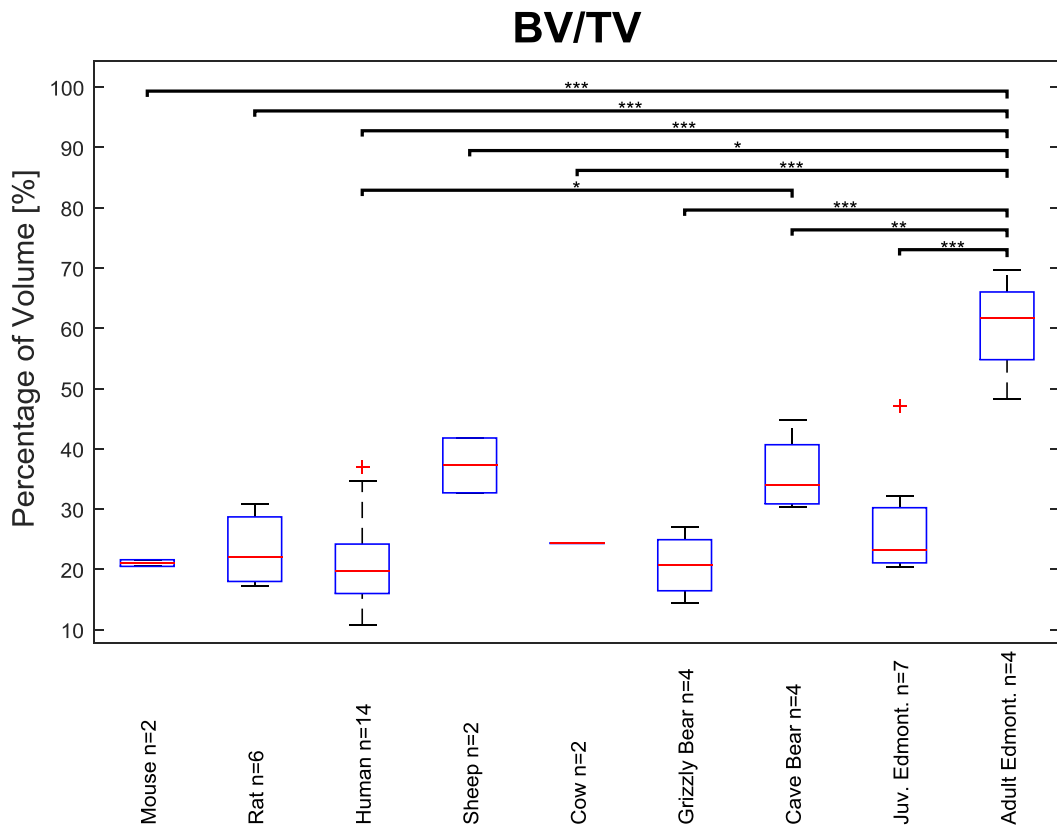


Figure 14: ANOVA of BV/TV comparing tibia BV/TV in 9 different species. Asterisks over bars represent levels of significance. One \* represents  $p < 0.05$ , Two \*\* represents  $p < 0.01$ , three \*\*\* represents  $p < 0.001$ . Red + represents outliers.

BV/TV was determined to not scale relative to body mass in mammals ranging in size from mouse to cow [55]. However, from the ANOVA of BV/TV, the adult edmontosaurus group measured significantly larger BV/TV compared from all other data groups ( $p < 0.0013$ ). Average BV/TV for adult edmontosaurs measured was 60.4%. The juvenile edmontosaurs samples only showed significant difference in BV/TV from the adult edmontosaurus group and had an average BV/TV of 27.1%.

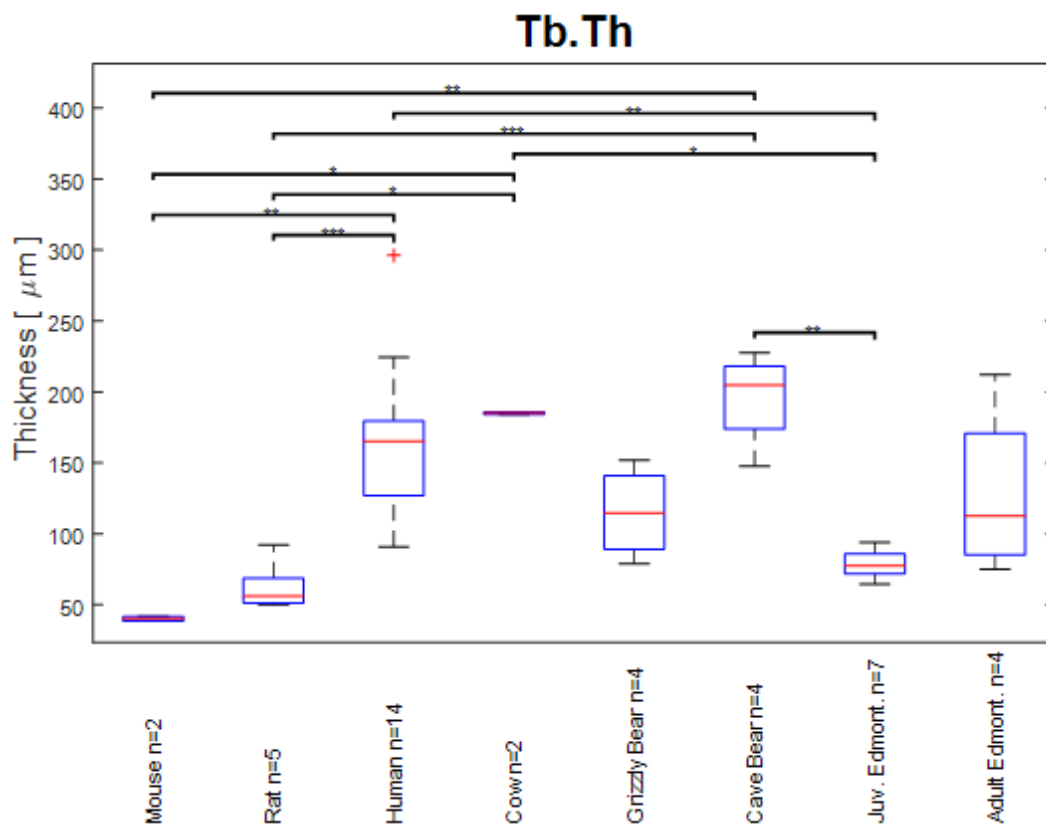
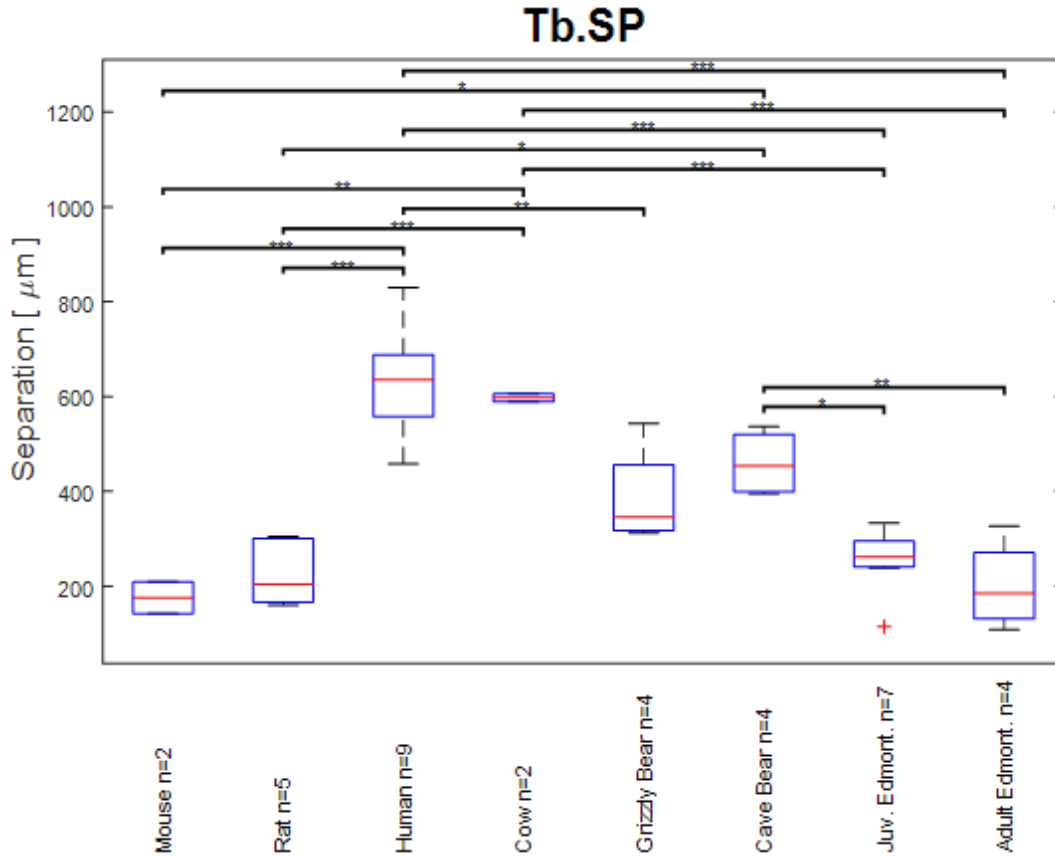


Figure 15: ANOVA of Tb.Th comparing tibia Tb.Th in 8 different species. Asterisks over bars represent levels of significance. One \* represents  $p < 0.05$ , Two \*\* represents  $p < 0.01$ , three \*\*\* represents  $p < 0.001$ . Red + represents outliers.

The Tb.Th of the adult edmontosaurs was not significantly different from any of the groups of tibia trabecular thickness data. The average Tb.Th measured from the 4 adult edmontosaurus bones was 127.9 microns. The average Tb.Th for the juvenile edmontosaurus

was 78.8 microns. Juvenile Tb.Th was significantly smaller than in humans, cows and cave bears ( $p < 0.0483$ ) while showing no differences from mice or rats.



**Figure 16: ANOVA of Tb.Sp comparing tibia Tb.Sp in 8 different species. Asterisks over bars represent levels of significance. One \* represents  $p < 0.05$ , Two \*\* represents  $p < 0.01$ , three \*\*\* represents  $p < 0.001$ . Red + represents outliers.**

Trabecular separation has been measured to increase with increasing body mass. However, in both adult and juvenile edmontosaurus samples measured, Tb.Sp was lower than expected. Tb.Sp in adult and juvenile edmontosaurs was measured to be significantly less than Tb.Sp measurements of cave bears, cows, and humans (adult  $P < 0.006$ ) (Juvenile  $P < 0.0175$ ). Tb.Sp was not measured to be significant between edmontosaurs of adult or juvenile age and mice or rats.

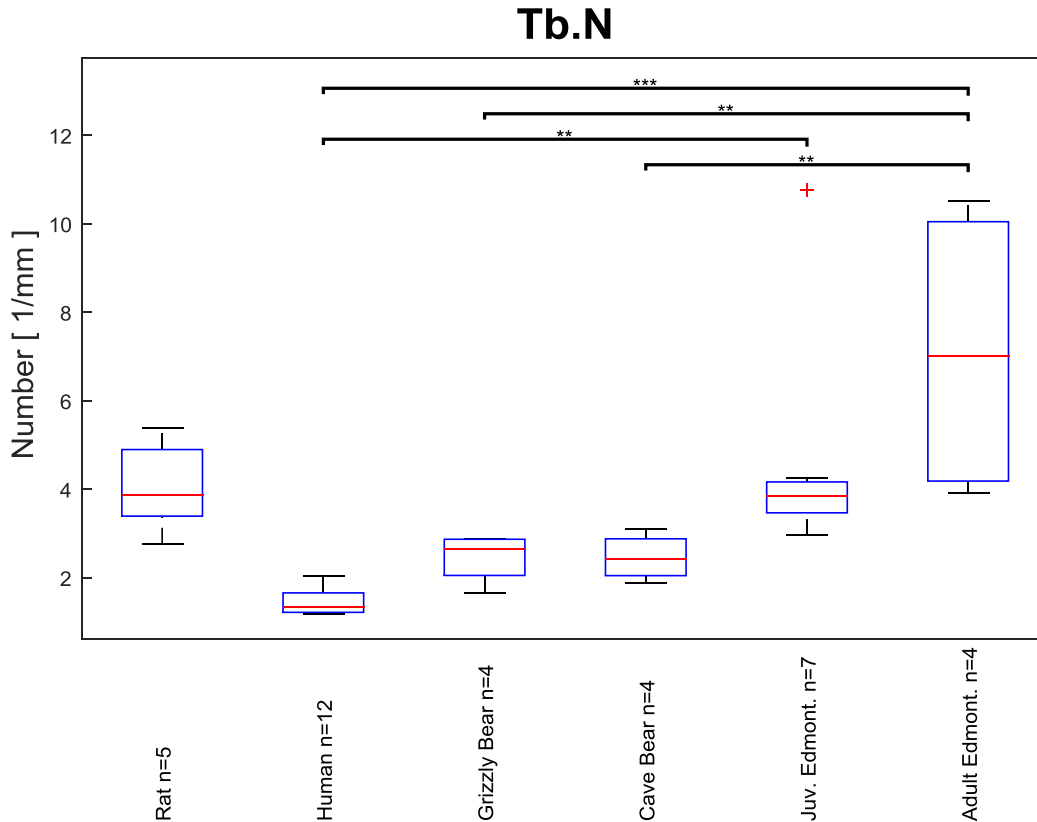


Figure 17: ANOVA of Tb.N comparing tibia Tb.N in 6 different species. Asterisks over bars represent levels of significance. One \* represents  $p < 0.05$ , Two \*\* represents  $p < 0.01$ , three \*\*\* represents  $p < 0.001$ . Red + represents outliers.

Tb.N in adult edmontosaurs, measuring an average of  $7.1 \text{ mm}^{-1}$ , was significant only compared to cave bears, grizzly bears and humans ( $p < 0.0063$ ). Tb.N in juvenile edmontosaurus samples measured an average of  $4.6 \text{ mm}^{-1}$  and showed significance only compared to humans ( $P = 0.0043$ ). Tb.N had the highest variance in measurement for the adult edmontosaurus samples. Sample variance is likely due to sedimentation within the sample that could not be fully filtered out of the evaluation region.

### 2.2.6 Edmontosaur Fossil Bone Verification

Due to the novelty of trabecular bone samples collected from fossils, there was some uncertainty as to the identity of the fossilized trabecular bone. In order to confirm the assumption that the material in the fossil trabecular bone cores was actually fossilized bone tissue, the

elemental composition of the fossils was examined. For this examination, the 7 juvenile edmontosaur samples were prepared for analysis in a JEOL JSM-6500F Scanning Electron Microscope (SEM) equipped with an Energy-dispersive X-ray Spectroscopy gun (EDS) (JEOL Ltd., Tokyo, Japan). An additional two samples were prepared from trabecular bone cores harvested from the C-1 vertebra from sheep (1 male, 1 female) as an extant bone control. It was also important to distinguish the fossilized bone from the surrounding rock, therefore, three samples were analyzed from surrounding rock matrix collected with the fossils. The bone core samples collected from the juvenile edmontosaurs and sheep were cut down into 4 mm tall cylinders using an IsoMet precision diamond saw (Buehler, Lake Bluff, Illinois). Core and matrix samples were coated in carbon prior to compositional analysis to facilitate conductivity of the samples in the SEM. Carbon coating was chosen for this application due to the near overlap of excitation energy seen between gold coating and calcium in samples. SEM EDS of bone tissue should reveal high relative compositions of calcium, phosphorus, and oxygen as those are major components in hydroxyapatite ( $\text{Ca}_{10}(\text{PO}_4)_6(\text{OH})_2$ ).

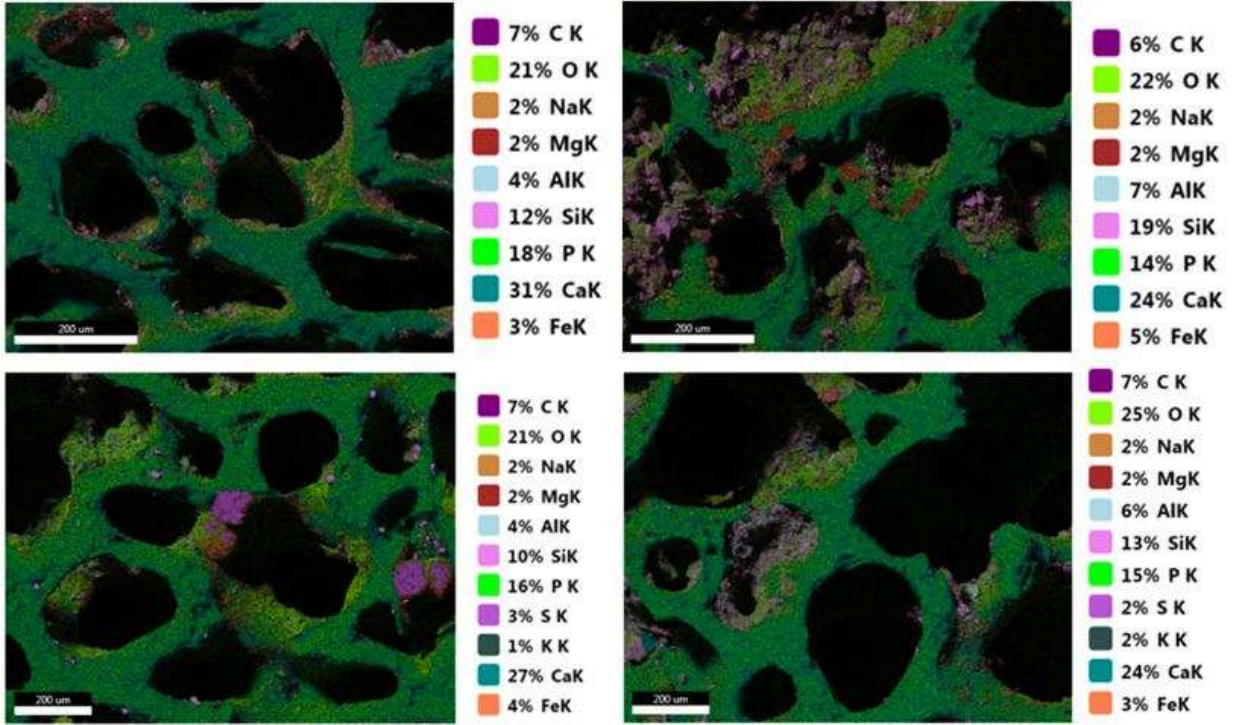


Figure 18: Example edmontosaur SEM EDS maps.

The relative composition maps of the juvenile edmontosaur samples showed a majority of compositional elements of Calcium, Phosphorous, Oxygen, Silicon, and Carbon. This is comparable to the sheep samples which were composed primarily of Calcium, Phosphorous, Oxygen, and Carbon.

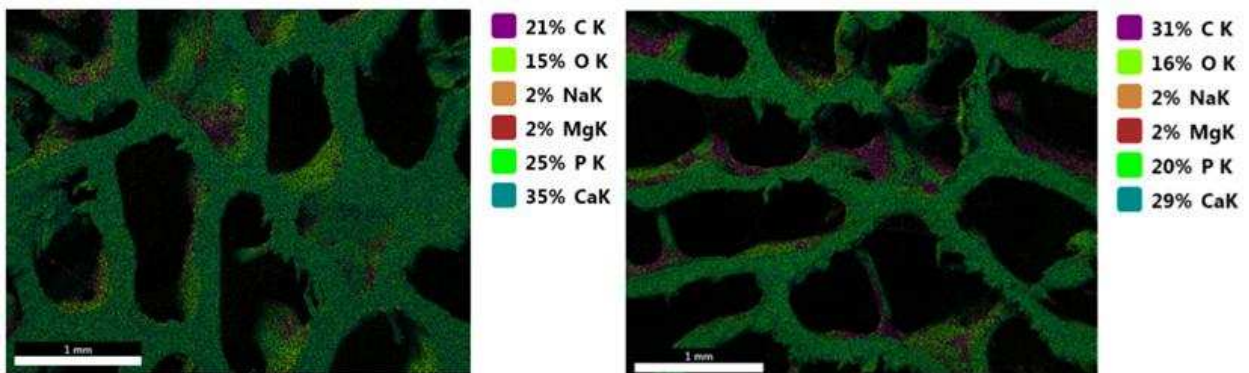


Figure 19: Sheep SEM EDS maps. Left: ewe. Right: ram

The relative compositions of the fossilized bone gives verification that what was sampled from these fossils is representative of the mineralized bone tissue that was grown and maintained by the animal during its life. The high concentrations of Silicon are likely due to sedimentation coming from the surrounding rock. This can be verified through the elemental compositions of the rock matrix samples. Calcium and Phosphorous do register in the rock matrix sample, but are not present as the dominant elements in the composition which are Aluminum, Oxygen, and Silicon. The low fractional percentage of Calcium and Phosphorous in the rock matrix indicate that the high fractional percentages of Calcium and Phosphorous in the fossilized bone likely did not come from the surrounding rock.

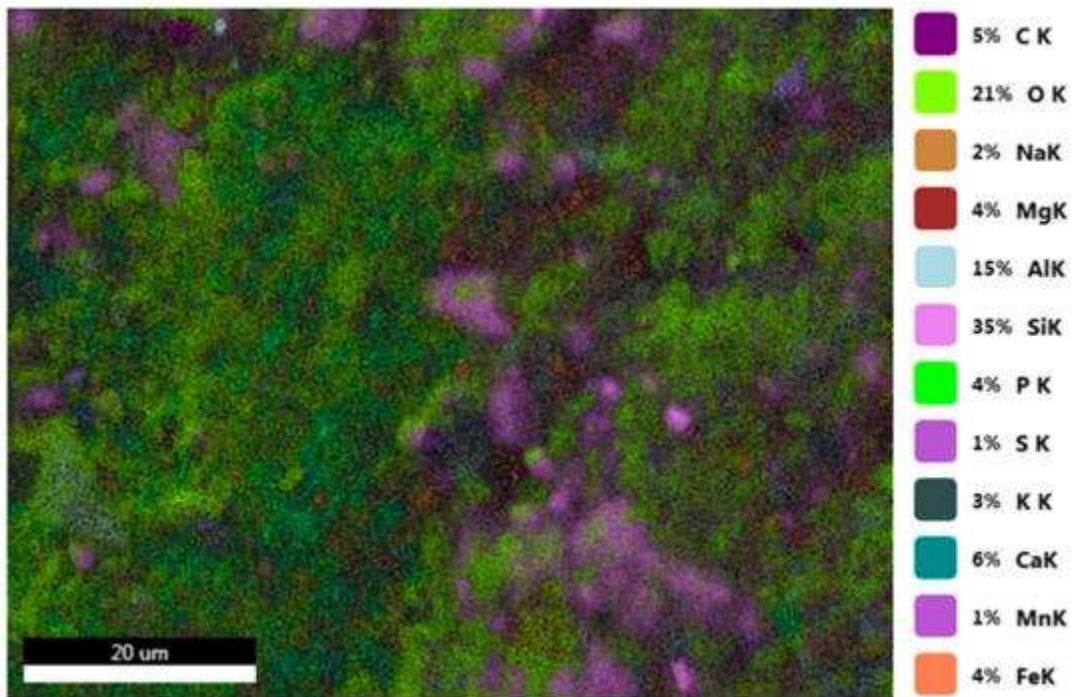


Figure 20: Rock matrix SEM EDS.

## **2.3 Bighorn Sheep Methods**

### **2.3.1 Bighorn Sheep Samples**

This research collected horn bone core images from 6 male bighorn sheep skulls. Skulls were sourced from road kill bighorn sheep ranging in approximate age from 3 to 8 years old. Bighorn sheep skulls used in this study were granted for research purposes by the state of Colorado Department of Natural Resources under Colorado Parks and Wildlife scientific collection license number 14SALV2052A2. This study also utilized the same 4 grizzly bear tibias utilized in the cave bear grizzly bear research for validation and as a trabecular bone control group.

### **2.3.2 Bighorn Sheep Sample preparation**

Bighorn sheep skulls were cleaned of soft tissues and stored frozen at -20 °C. Prior to imaging, skulls were removed from the freezer and set out to thaw for a 12 hour period. The curl length of each horn was measured from the base of the horn keratin sheath to the horn tip using a string aligned along the outer circumference of the horn. The 4 grizzly bear tibias had 8 mm diameter core samples drilled from the proximal end of the tibia. The drilling location for these cores was located within the medial portion of the lateral condyle. Bone cores were cut from the tibias using a diamond sintered coring drill bit and a desktop band saw. Grizzly bear core samples ranged in length from ~15 to ~25mm.

### **2.3.3 Bighorn Sheep Sample Imaging**

The bighorn sheep horn cores were too large to image using the SCANCO  $\mu$ CT 80, so the full skulls were imaged in the Gemini Time-of-Flight Big Bore PET/16 slice CT (Philips Healthcare, Andover, MA) machine at the Colorado State University Veterinary Teaching Hospital. The smaller sheep skulls were scanned facing parallel to the PET/CT scan direction, while larger skulls were turned perpendicular to the PET/CT scan direction. Skulls were turned

because the horns on the larger samples prevented the skulls from fitting inside the PET/CT gantry when aligned parallel to the scan direction. Scan images measured by the PET/CT machine were separated by a slice thickness of 1mm. The grizzly bear core samples were imaged in a SCANCO  $\mu$ CT 80 machine. The imaged region included a 2 mm tall volume approximately 1 to 2 mm proximal to the physis. Images of the grizzly bear cores were recorded at medium resolution resulting in 20 micron voxels.

#### **2.3.4 MATLAB Code Formulation**

A MATLAB script program was written to measure the bone morphological parameters for velar bone volume fraction (BV/TV), thickness (V.Th), separation (V.Sp), and number (V.N) of the bighorn sheep horn cores. Before bone morphological property measurements could be performed, the image series recorded using the PET/CT required image processing as a result of scanning methodology. Image processing included voxel squaring, using linear interpolation between slices, and volume of interest and image thresholding determination through user input. Image thresholding determined which voxels corresponded to solid volume and which voxels corresponded to non bone volume (pore space).

The bone volume fraction parameter was determined by dividing the total number of solid voxels by the number of total voxels within the designated volume of interest. Morphological calculations for bone thickness and bone separation implemented the Hildebrand and R uegsegger method for model independent assessment of thickness and spacing [79,80]. Through this method, maximal spheres are fit to each voxel point within a 3-dimensional object. Initial diameter values for iteration were assessed using a 3-dimensional distance transformation between bone voxels. All voxels were then assigned a value for separation and thickness measurements corresponding to the diameter of the maximal sphere which could fill the void

space or bone volume respectively. Morphological parameters were then determined by averaging the maximal diameter values assigned to the corresponding voxels. Bone separation was determined using diameter values of voxels corresponding to non solid volume, while bone thickness measurements were averages of diameter values of all voxels corresponding to solid volume. The bone number morphological parameter measurements were derived by averaging the diameter values from a 3-dimensional distance transformation on a skeletonized transformation of the solid volume.

### **2.3.5 MATLAB Code Validation**

The MATLAB bone measurement script program used in measuring the BV/TV, V.Sp, V.Th, and V.N parameters was validated using the dicom images of the 4 grizzly bear cores at 20 micron resolution. Trabecular bone properties were calculated for the 4 grizzly bear core samples using the SCANCO proprietary software. All volumes of interest were drawn to exclude the outer 100-200 microns of the trabecular bone cores to avoid including possible damage due to sample preparation in the analysis volume. Sample thresholding was determined by the measurement program operator to be the threshold where binary bone masking most closely matched a visual inspection of the bone in the DICOM image. The DICOMS from the  $\mu$ CT scans used in the SCANCO trabecular bone evaluation were uploaded into the MATLAB analysis. The methods used to determine the volume of interest and image thresholding in the SCANCO software were applied to the MATLAB analysis as well. Measurements for BVTV, Tb.Sp, Tb.Th, and Tb.N were calculated and stored. Final results of each method were compared using a t-test between the SCANCO evaluation and MATLAB evaluation.

### **2.3.6 Bighorn Sheep horn and horn core measurements**

The images from the PET/CT imaging machine were uploaded into MATLAB. Each image stack was scaled using linear interpolation between slices to square the voxels from

rectangular prisms into cubic volumes. Bighorn sheep horn core region of interests were drawn to include all image voxels from the base of the anatomical right horn to the tip of its corresponding horn core excluding voxels outside 1-2 mm within the cortical wall (fig 21). The image threshold was determined using the same operator based visual method used in the MATLAB validation tests. Values for BVTV, V.Sp, V.Th, and V.N were measured and recorded.

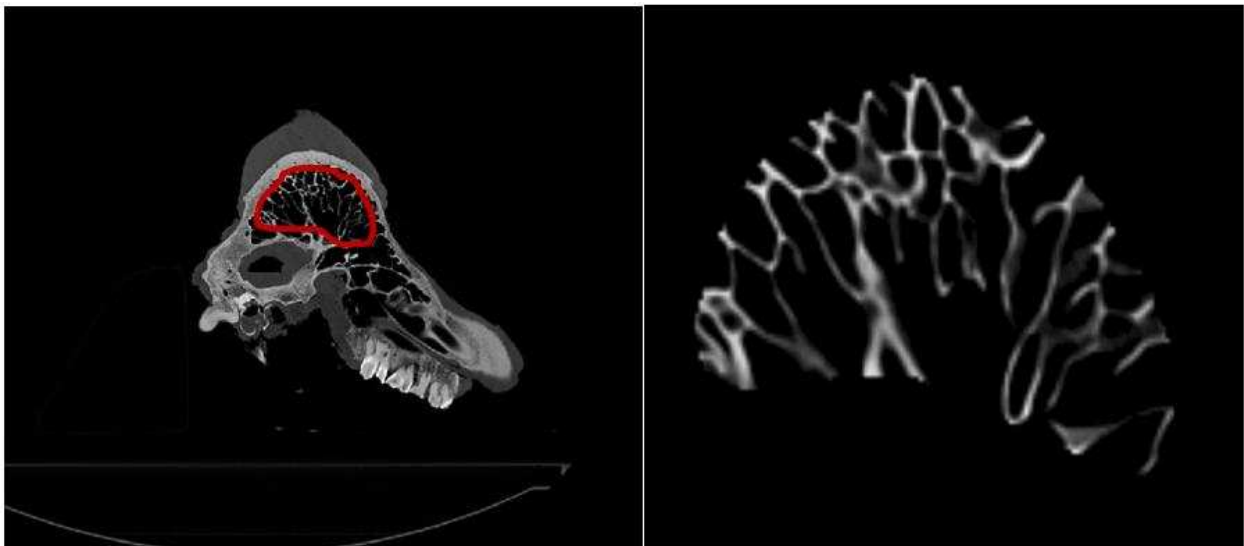


**Figure 21: Bighorn sheep CT ROI selection.**

Horns of bighorn sheep are not shed year to year like antlers. Therefore, the size of a rams horns is an indication of the age and size of the sheep. Larger sheep presumably, could generate greater forces during impact further affecting the structural morphology of their horn core velar bone. Horn size was measured for each sample using a string and wrapping it along the outer circumference of the horn from the base of the horn to the tip. The string length from base to tip was recorded in cm using a tape measure.

### **2.3.7 Bighorn Sheep Statistics**

The MATLAB evaluation of morphological bone properties was validated using a one-tailed t-test on the measured parameters. A result of no significance between the created MATLAB evaluation and SCANCO evaluation software validates the accuracy of the created evaluation. Horn core bone properties were compared against the grizzly bear tibial trabecular bone core samples using two-sample t-tests at a 95% confidence interval for each parameter of measurement. Horn core bone properties were also compared as a function of curl length using linear regression.

### **2.3.8 Bighorn Sheep Results**

The parameters for BV/TV, Tb.Th, Tb.Sp, and Tb.N were not significant between the MATLAB and SCANCO evaluation methods validating the use of the MATLAB evaluation for accurate measurements of velar morphological properties ( $P > 0.05$ ).

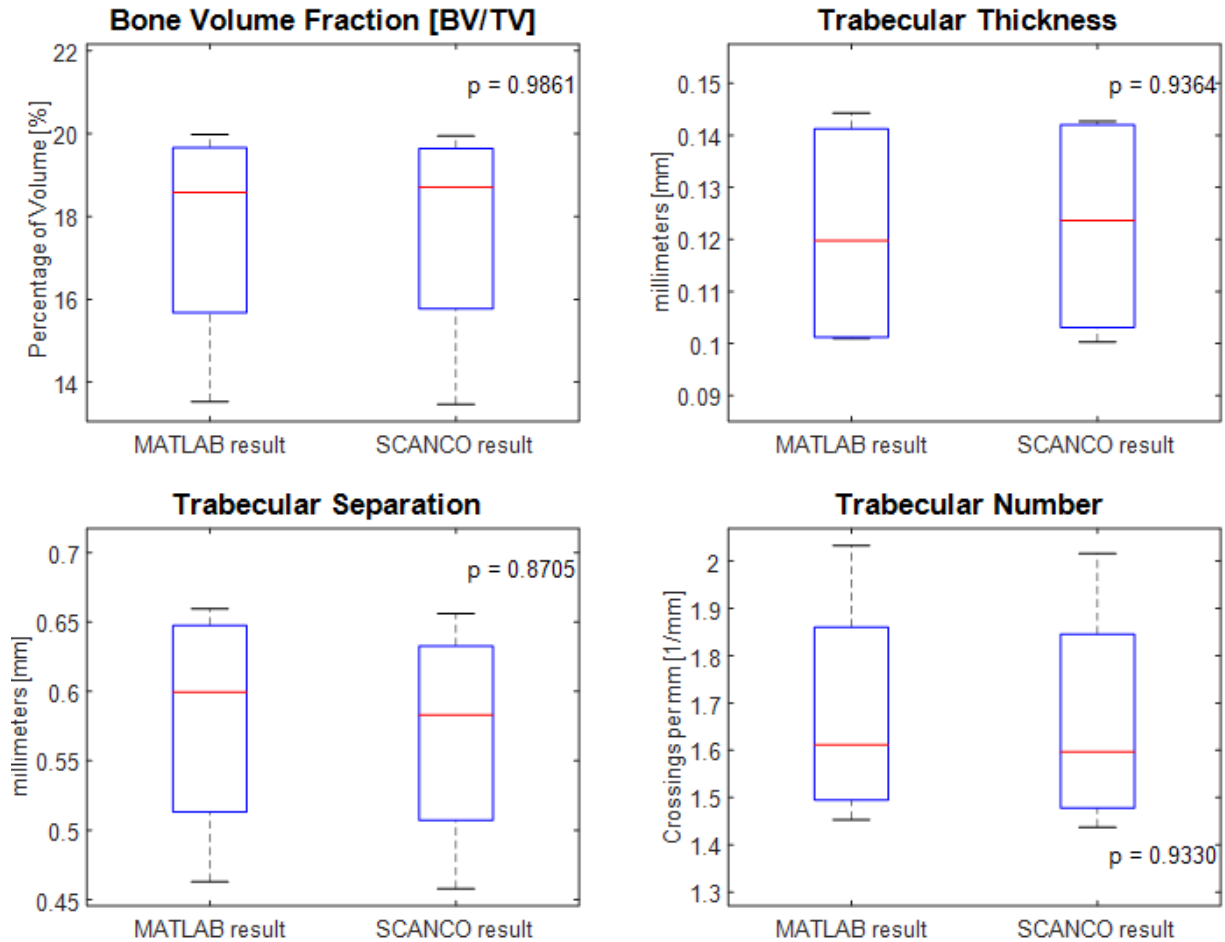


Figure 22: MATLAB evaluation validation t-tests.

The comparison of velar bone morphological properties to grizzly bear trabecular bone properties is shown in figure 22. The measurements of BV/TV were not found to be significant between horn core velar bone and trabecular bone. However, V.Th, V.Sp, and V.N were all found to be significant between bighorn sheep horn core velar bone and grizzly bear trabecular bone. Velar bone struts were measured with an average thickness of  $2.87 \pm 0.78$  mm. This is 26 times thicker than trabecular bone struts which were measured at an average thickness of  $0.12 \pm 0.02$  mm. The velar number was measured at an average of  $0.09 \pm 0.009$  sails per mm compared

to an average of  $1.66 \pm 0.25$  struts per mm measured in grizzly bear trabecular bone. The velar separation was measured at an average distance of  $11.91 \pm 0.88$  mm which is nearly 21 times greater than the separation measured between the bone struts in grizzly bear trabecular bone with an average separation of  $0.57 \pm 0.08$  mm.

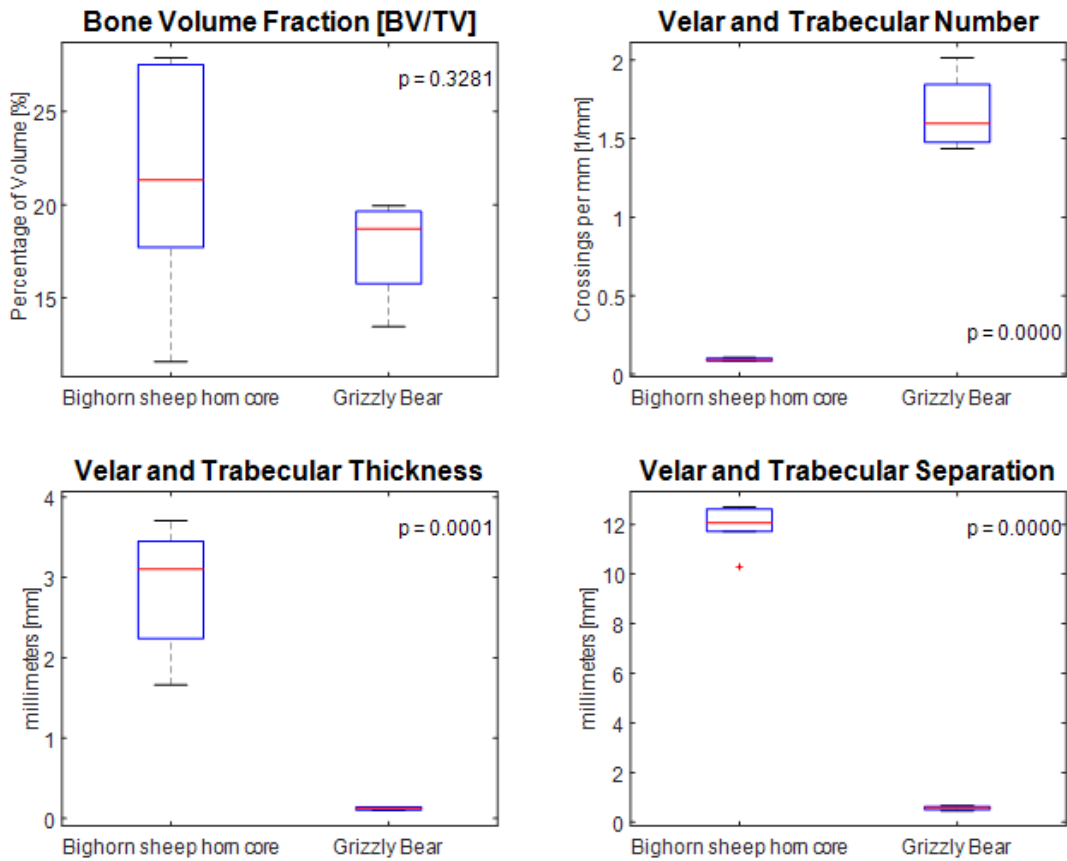


Figure 23: Velar and trabecular bone property measurement comparisons.

Plots of bone properties against curl length show trending properties of horn core velar bone with horn curl length. BV/TV, V.Th, V.N were all found to significantly increase with increasing horn curl length. The V.Sp regression was not significant but shows a potential decreasing correlation with increasing curl length which could be confirmed through additional sampling.

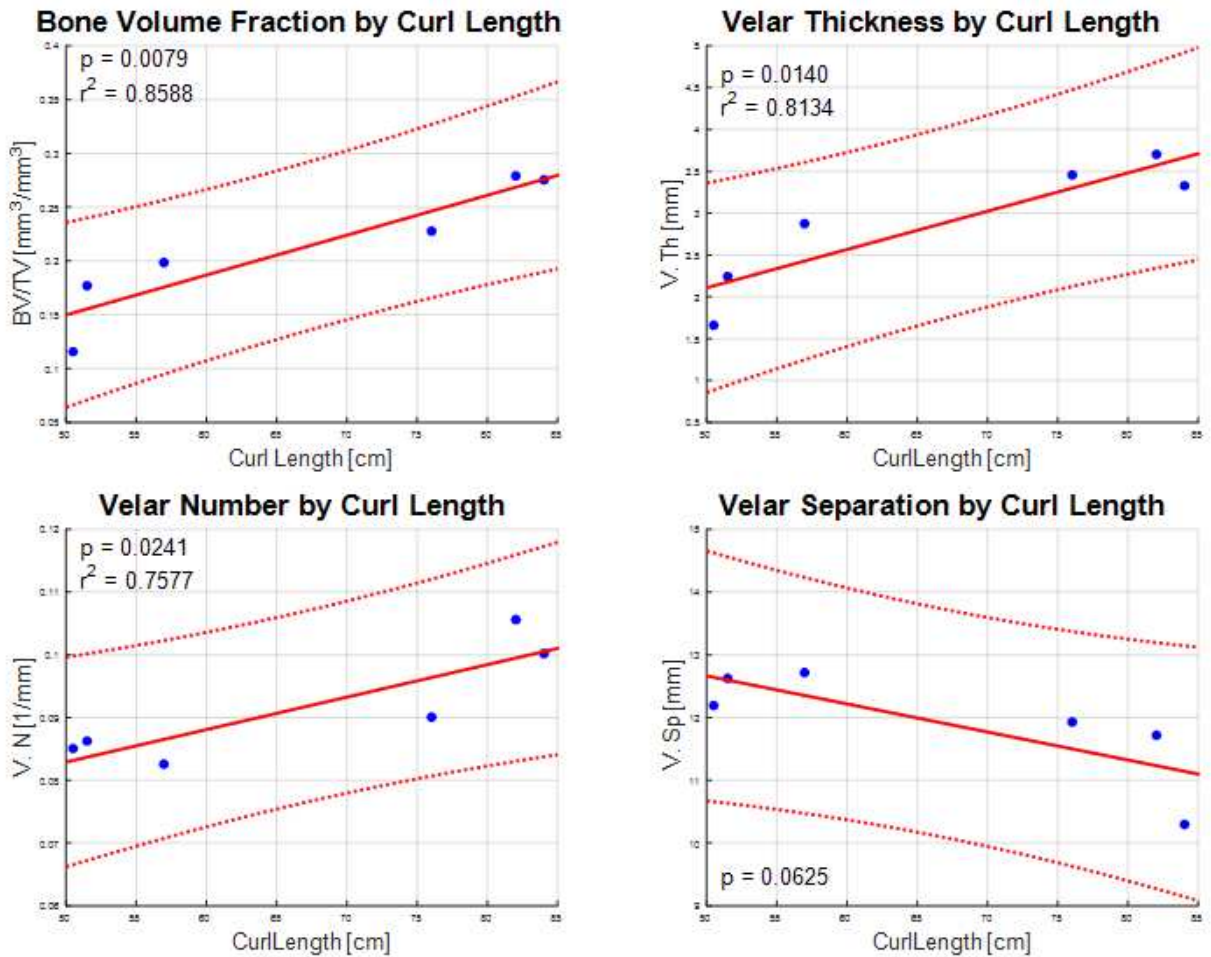


Figure 24: Linear regression plots of velar properties by horn curl length. Dashed lines show the 95% confidence bounds of each regression.

## **Chapter 3: Discussion**

### **3.1 Cave Bear and Grizzly Bear Discussion**

In recent history, grizzly bears have been well studied for their unique ability to resist disuse bone resorption in trabecular bone during long periods of inactivity. Cave bears, an extinct near relative of modern day grizzly bears, have not been as extensively studied. Specifically, the examination of cave bear trabecular bone morphology is a novel exploration in this research. Based on fossil record, cave bears are expected to be nearly 84% larger, by body mass, than their surviving grizzly bear relatives. In this research, cave bears were expected to have the same bone volume fraction, greater trabecular thickness and separation, and lower trabecular number than grizzly bears due to the estimated difference in body weight between the two species.

Experimental results from this study did not fully corroborate with the hypothesis. The significantly greater Tb.Th in cave bear was an expected result due to the difference in average size between grizzly bears and cave bears. However, the significance in BV/TV was a somewhat surprising result for the cave bears. According to published body mass scaling relationships, there is no significant scaling relationship between BV/TV and total body mass. This lack of scaling is likely because the increase in Tb.Sp and decrease in Tb.N with increasing body mass balance out the bone volume addition from increased Tb.Th. Cave bear trabecular bone showed no significant differences in Tb.Sp or Tb.N compared to grizzly bears despite their differences in body mass. Considering that the cave bear trabecular bone measurements showed no differences in Tb.Sp and Tb.N but a significant increase in Tb.Th, it is reasonable that BV/TV increased as well. An increase in Tb.Th without a decrease in Tb.Sp or Tb.N represents an increase in the average bone volume of each trabecular strut. Without a compensating decrease in Tb.N or an

increase in the Tb.Sp, the void space of the bone is not similarly increased. This results in a greater BV/TV.

The increase in Tb.Th and BV/TV in cave bear trabecular bone could be a possible indication of a few different functional roles of trabecular bone in cave bears. Firstly, it is unknown whether cave bears shared a similar inhibition towards bone resorption during hibernation as seen in extant bears. Without the biochemical inhibition to bone resorption, an increase in Tb.Th could have been a physiological preparation for inactivity. In effect, this could have been similar to the way that hibernating animals store up fat prior to hibernation. In the case of trabecular bone this would be exhibited in the storing up of bone volume so that during the period of inactivity, bone resorption would not weaken the bone beyond functional use. The second case for increased BV/TV and Tb.Th is that cave bears could have adapted thicker trabeculae from the Etruscan bear in comparison to grizzly bears. This model for suggesting differences in bone adaptation could better be explored by sampling trabecular bone in ancestors to the grizzly bear dating back to the Etruscan bear.

It is possible that the potential for bioinspired material design stemming from the cave bear trabecular bone morphology could not be as useful as the design stemming from the edmontosaurus or bighorn sheep bone porous bone structures. The cave bear trabecular bone morphology follows a similar trend to the edmontosaurs in that the BV/TV was larger than expected from published body mass scaling relationships [55]. However, the edmontosaurs have a more impactful result on a bioinspired design due to their enormous body mass advantage over cave bears. Alternatively, studying cave bear trabecular bone could be more advantageous than edmontosaurs in analyzing potential mechanical material property changes over time. The near ancestry of cave bears and grizzly bears makes it easier to study the differences in potential

evolutionary adaptations in mechanical compressive loading studies. Additionally, dinosaur fossils are difficult to find and can take years to extract from surrounding rock matrix. These disadvantages in fossil study and collection make some researchers reluctant to allow destructive processes when studying dinosaurs.

### **3.2 Dinosaur Discussion**

The study of dinosaur trabecular bone is a novel and potentially groundbreaking concept in biomechanics research. Under the consideration of Wolff's law, dinosaur trabecular bone was optimized through bone remodeling processes to withstand massive loads on a regular basis. From human study it is known that hip joint forces during basic ambulation can measure up to several times the total body weight. Applying a similar thought process to dinosaur bones means that adult dinosaur bone could routinely withstand loads in ranges of the 100's of kN [68]. Bone utilizes both trabecular and cortical bone to gain mechanical advantage and distribute force to reduce maximal internal stress. Therefore, the high load environment on trabecular bone as a result of gigantism will drive bone morphology to maintain optimal levels of bone strain in vivo. The hypothesis of this research was that edmontosaurs trabecular bone will exhibit specialized morphology utilizing comparable BV/TV, high Tb.Th and Tb.Sp, and low Tb.N as compared to extant animals. In actuality, the trabecular bone morphology of the sampled edmontosaurs did not follow what was expected in the hypothesis.

According to body mass scaling relationships in trabecular bone, as an animal's body mass increases the trabecular bone becomes occupied by less numerous, thicker and more widely separated trabeculae [50]. The juvenile edmontosaurs trabecular bone showed indications that the trabecular bone might increase in BV/TV as the animal aged. This increase in BV/TV might be a growth response in the bone to compensate for increased bone forces with increasing body mass.

Trabecular bone in the adult edmontosaurs was characterized not according to the expected body mass scaling relationships, but by more numerous, thin, and tightly packed trabeculae leading to bone with significantly greater BV/TV than expected. Trabecular bone properties measured in cows averaging approximately 600 kg have average reported BV/TV of 24.3%, average Tb.Th of 185 microns, average Tb.Sp of 597 microns, and 1.5 trabecular struts per mm. Adult edmontosaurs, averaging approximately 8,000kg, would be expected to have even greater Tb.Th and Tb.Sp and lower Tb.N than that of cows based on body mass scaling relationships. However, the measurements collected in this research show the opposite effect with adult edmontosaurs having smaller Tb.Th, and Tb.Sp with larger Tb.N compared to these large terrestrial mammals. In birds and reptiles, trabecular bone properties have been compared to femoral head radius showing increasing Tb.Th and Tb.Sp with increasing femoral head dimensions. Dinosaurs, despite being evolutionary ancestors to extant birds, did not agree with what would be expected based on allometric scaling relationships in birds [81]. Additionally, bird BV/TV was measured and reported at an average of  $0.19 \pm 0.01$  which is much smaller than the measured values for adult edmontosaurs. However, bird BV/TV did show some weak positive correlation with increasing femoral condyle size. The greater BV/TV in edmontosaurs makes some sense mathematically in that it has the theoretical ability to support greater stress as a cellular solid due to increasing elastic modulus of the structure[82].

Stated previously in section 1.3, cellular solids continuum material properties are dependent on the material of the struts, the shape and topology, and the relative density of the foam [25]. Due to the fossilization process, there are limitations to knowing that the morphology of trabecular bone within a fossil is accurate to the in vivo bone of the animal. These limitations are reduced through SEM EDS relative chemical composition analysis which showed that bone

strut material was consistent with chemical compositions of hydroxyapatite in both extinct and extant animals. The similarity in chemical composition also indicates that bone material is an unlikely primary contributor in the ability of dinosaur trabecular bone to accommodate the loads associated with gigantism. The shape and topology of the edmontosaurs trabecular bone was different than hypothesized based on body mass scaling relationships. However, the edmontosaurus insignificance in Tb.Th, and Tb.Sp from extant mammals indicate that shape and topology was also an unlikely primary contributor in withstanding the forces of gigantism. Relative density of a cellular solid is a strong contributor to continuum properties and could be a driving mechanical factor in edmontosaurs trabecular bone. As the volume fraction of a foam increases, the properties of the continuum material become more similar to that of the solid non-porous material. So, greater trabecular BV/TV would result in greater elastic modulus of the trabecular volume[82]. Mathematically, the stress ( $\sigma$ ) on a porous material in axial compression can be given by the following equation where E is the elastic modulus and  $\epsilon$  is the resultant strain on the material.

$$\frac{\sigma}{E} = \epsilon$$

This means that a stress applied to two cellular solids of varying fractional density, would result in different strains where the greater volume fraction material would have lesser resultant strain. This continuum material adaptation can be seen in the significantly increased trabecular bone volume fraction of the adult edmontosaurs. Therefore, it is likely that the increased bone volume fraction of the edmontosaurs trabecular bone is the primary contributor to the ability of trabecular bone to support the massive forces associated with gigantism in animals.

Through this research, trabecular bone was proven to be a measurable and unique bone structure in fossilized dinosaur bones. This work has pioneered a new potential candidate for bioinspired material design of optimized foams or structures for high force applications. This research cannot conclusively prove the effect of dinosaur trabecular bone in maintaining in vivo microstrain within the 2,000 to 3,000 microstrain target determined by dynamic strain similarity. Trabecular bone is only a small portion of the total bone and its complex structure adapted for accommodating mechanical loads. Trabecular bone works in concert with cortical bone size, geometry, and curvature to distribute applied stress. Therefore, future research could further isolate the contribution of edmontosaur trabecular bone to the mechanical response through compression testing of trabecular bone mimics. Compressive loading simulation and testing between trabecular bone structures replicated from dinosaurs, large extant animals, such as cow or elephant, and engineered foams, such as polyurethane, would provide additional insight into the capability of dinosaur trabecular bone to distribute such large forces. Future work in creating a mimic or bioinspired foam based on the edmontosaurus trabecular bone morphological properties could have applications wherever high strength to weight ratio properties are desired.

### **3.3 Bighorn Sheep Horns Discussion**

Bighorn sheep velar bone in the horn core of male bighorn sheep represents porous bone adapted to high impact loading. During rut, male bighorn sheep compete for mating rights through repeated ramming events. In a single ramming event, impact velocities up to 6 m/s have been measured with decelerations up to 34 m/s<sup>2</sup>. This deceleration in the animal translates to an estimated 3400N load, assuming the ram weighs 100kg, which appears to result in no lasting damage to the ram. Previous research into bighorn sheep horns during impact analyzed rotational brain cavity accelerations using finite element model impact simulations with and without the

porous velar bone inside the horn core [75]. When the velar horn core bone was removed from the analysis, brain cavity accelerations reportedly increased by 442% compared to the simulation with velar bone material intact. These results suggest that bighorn sheep horn core bone fulfills a significant role in absorbing energy and mitigating brain damage from repeated high impact events experienced by male bighorn sheep during mating rituals. Horn core velar bone has likely functionally adapted through the principles described by Wolff's law and mechanotransduction to optimally respond to intermittent high impact forces as opposed to the low impact environment of trabecular bone in long bones. It was hypothesized that bighorn sheep horn core velar bone adapted morphological properties for BV/TV, V.Th, V.Sp, V.N, to be significantly different from trabecular bone properties common to long bones. These adapted properties were expected to be different in response to the high impact loading environment of bighorn sheep horns compared to quasi-static compression dominated loading of trabecular bone in long and flat bones.

From visual inspection (fig 3) and the morphological parameters quantified here (fig 22), it is clear that the velar bone in the bighorn sheep horn core is organized with a different structural architecture than trabecular bone. The sail-like bone formations of the velar bone appear to be composed of fewer numbered, more widely separated, and thicker bone formations than trabecular bone. The average V.Th was surprisingly thick at 2.88 mm. This V.Th is 26 times greater than grizzly bear Tb.Th at an average Tb.Th of 0.122 mm. Velar separation averaged V.Sp 11.91 mm between velar sails, which is nearly 21 times greater than Tb.Sp of grizzly bear trabecular bone at an average Tb.Sp of 0.57 mm. Velar number was measured at nearly 18 times less frequent than Tb.N in grizzly bears given average V.N of  $0.09 \text{ mm}^{-1}$  for bighorn sheep horn core and average Tb.N of  $1.66 \text{ mm}^{-1}$  in grizzly bear trabeculae. Notably,

measured BV/TV in velar bone is not significant from BV/TV measured in grizzly bear trabecular bone despite the thick velar sails.

The extremely high thickness and separation of the velar bone is likely an adaptation of the horn core velar sails to mitigate stress in bending. Simple bending stress is given by equation shown below where  $M$  is the incident moment,  $Y$  is the distance from the neutral axis, and  $I$  is the area moment of inertia of the cross section.

$$\sigma = \frac{M * Y}{I}$$

Based on the equation for simple bending, stress on an object loaded in bending can be reduced by reducing the incident moment, reducing the maximal distance from the neutral axis, and/or increasing the moment of inertia of the object. An object's moment of inertia is increased by moving mass away from its center of gravity such as thickening the bone in the velar sails and increasing separation between the velar sails. This is a common principal in engineered construction beams. For example, I-beams are designed so mass is distanced from the neutral axis in order to reduce peak stress in a beam without requiring the addition of more material. Due to the large thickness and separation of the bone sails the horn core as an entire structure must be examined in order to consider velar horn core bone as a cellular solid material. The structural properties of velar bone are likely governed by the potential modification of material morphology rather than modifications to the relative density as seen with the edmontosaur trabecular bone. The assessment that the continuum properties of velar bone as a cellular solid is dominated by the shape and morphology is further backed by the lack of difference in BV/TV between velar bone and trabecular bone. If the structure of velar bone was unimportant to energy

absorption in bighorn sheep horns, it would be possible that the horns would instead be filled with bone structure similar to trabecular bone rather than velar bone structure.

Adapting bone morphology for energy absorption would be important functionally for bone under repeated incidents of high impact loading, as in bighorn sheep horn core bone. As discussed previously, the horns of bighorn sheep are not shed and re-grown each season, like the antlers of elk or deer. This means that damage accumulated through ramming cannot be reversed through the shedding and re-growth of the horns. Due to the secondary remodeling processes of bone, it is an advantageous biological material for energy absorption in horns [22-24]. This remodeling process extends the plateau region of plastic collapse in the stress strain curve indicative of cellular solids by rebuilding damaged bone. Extending potential plastic collapse increases the total strain energy density of the horn by removing cracks and decreasing the opportunity for catastrophic failure.

The work presented by this research on velar bone morphology is currently being expanded upon by other members of the bone biology and mechanics research laboratory led by Dr. Seth Donahue. Sections of the horn core velar bone are being mimicked using additive manufacturing techniques. Additionally, bioinspired foam designs have been created based on quantified velar morphology data collected using the MATLAB evaluation developed in this research. Mechanical impact testing of these bioinspired and bio-mimicked foam materials may reveal novel foam structure designs useful for products requiring high energy absorption materials.

## References

1. Meyers, M.A., et al., Biological materials: Structure and mechanical properties. *Progress in Materials Science*, 2008. 53(1): p. 1-206.
2. Aoyagi, Seiji, et al. "Biodegradable Polymer Needle with Various Tip Angles and Consideration on Insertion Mechanism of Mosquito's Proboscis." *Sensors and Actuators A: Physical*, vol. 143, no. 1, 2008, pp. 20–28., doi:10.1016/j.sna.2007.06.007.
3. Chen, P.Y., et al., Structure and mechanical properties of selected biological materials. *Journal of the Mechanical Behavior of Biomedical Materials*, 2008. 1(3): p. 208-226.
4. Burr, D.B., The contribution of the organic matrix to bone's material properties. *Bone*, 2002. 31(1): p. 8-11.
5. Office of the Surgeon General (US). *Bone Health and Osteoporosis: A Report of the Surgeon General*. Rockville (MD): Office of the Surgeon General (US); 2004. 2, The Basics of Bone in Health and Disease. Available from: <https://www.ncbi.nlm.nih.gov/books/NBK45504/>
6. Rinaldo Florencio-Silva, Gisela Rodrigues da Silva Sasso, Estela Sasso-Cerri, Manuel Jesus Simões, and Paulo Sérgio Cerri, "Biology of Bone Tissue: Structure, Function, and Factors That Influence Bone Cells," *BioMed Research International*, vol. 2015, Article ID 421746, 17 pages, 2015. doi:10.1155/2015/421746
7. Wang, Xiaodu, et al. "The role of collagen in determining bone mechanical properties." *Journal of orthopaedic research* 19.6 (2001): 1021-1026.
8. Sasaki, Naoki, and Singo Odajima. "Stress-strain curve and Young's modulus of a collagen molecule as determined by the X-ray diffraction technique." *Journal of biomechanics* 29.5 (1996): 655-658.
9. Currey, John D. "The relationship between the stiffness and the mineral content of bone." *Journal of biomechanics* 2.4 (1969): 477-480.
10. Gilmore, R. S., and J. L. Katz. "Elastic properties of apatites." *Journal of Materials Science* 17.4 (1982): 1131-1141.
11. Bembey, A.K., et al., Hydration effects on the micro-mechanical properties of bone. *Journal of Materials Research*, 2006. 21(8): p. 1962-1968.
12. Currey, J.D., Effects of differences in mineralization on the mechanical properties of bone. *Philos Trans R Soc Lond B Biol Sci*, 1984. 304(1121): p. 509-18.
13. Carter, D.R. and W.C. Hayes, Bone compressive strength: the influence of density and strain rate. *Science*, 1976. 194(4270): p. 1174-6.
14. Linde, F., et al., Mechanical properties of trabecular bone. Dependency on strain rate. *J Biomech*, 1991. 24(9): p. 803-9.

15. Schaffler, M.B., E.L. Radin, and D.B. Burr, Mechanical and morphological effects of strain rate on fatigue of compact bone. *Bone*, 1989. 10(3): p. 207-14.
16. Brodt, M.D., C.B. Ellis, and M.J. Silva, Growing C57Bl/6 mice increase whole bone mechanical properties by increasing geometric and material properties. *J Bone Miner Res*, 1999. 14(12): p. 2159-66.
17. Martin, R.B. and D.L. Boardman, The effects of collagen fiber orientation, porosity, density, and mineralization on bovine cortical bone bending properties. *J Biomech*, 1993. 26(9): p. 1047-54.
18. Martin, R.B. and J. Ishida, The relative effects of collagen fiber orientation, porosity, density, and mineralization on bone strength. *J Biomech*, 1989. 22(5): p. 419-26.
19. Sedlin, E.D. and C. Hirsch, Factors affecting the determination of the physical properties of femoral cortical bone. *Acta Orthop Scand*, 1966. 37(1): p. 29-48.
20. Parfitt, A. M., Drezner, M. K., Glorieux, F. H., Kanis, J. A., Malluche, H., Meunier, P. J., Ott, S. M. and Recker, R. R. (1987), Bone histomorphometry: Standardization of nomenclature, symbols, and units: Report of the asbmr histomorphometry nomenclature committee. *J Bone Miner Res*, 2: 595–610. doi:10.1002/jbmr.5650020617
21. Paluch, E.K., et al., Mechanotransduction: use the force(s). *BMC Biol*, 2015. 13: p. 47.
22. Hadjidakis, D.J. and Androulakis, II, Bone remodeling. *Ann N Y Acad Sci*, 2006. 1092: p. 385-96.
23. Verborgt, O., G.J. Gibson, and M.B. Schaffler, Loss of osteocyte integrity in association with microdamage and bone remodeling after fatigue in vivo. *J Bone Miner Res*, 2000. 15(1): p. 60-7.
24. Robling, A.G., A.B. Castillo, and C.H. Turner, Biomechanical and molecular regulation of bone remodeling. *Annu Rev Biomed Eng*, 2006. 8: p. 455-98.
25. Bergmann G, Deuretzbacher G, Heller M, et al. Hip forces and gait patterns from routine activities. *J Biomech*. 2001;34: 859–871. [http://dx.doi.org/10.1016/S0021-9290\(01\)00040-9](http://dx.doi.org/10.1016/S0021-9290(01)00040-9) pmid:11410170
26. Ashby, M. F., et al. "The mechanical properties of natural materials. I. Material property charts." *Proc. R. Soc. Lond. A*450.1938 (1995): 123-140.
27. Cameron, John R.; James G. Skofronick & Roderick M. Grant. *Physics of the Body*. Second Edition. Madison, WI: Medical Physics Publishing, 1999: 96.
28. Pal, Subrata. *Design of Artificial Human Joints & Organs*. Springer-Verlag New York, 2016.
29. Biewener, Andrew A. "Mammalian Terrestrial Locomotion and Size." *BioScience*, vol. 39, no. 11, 1989, pp. 776–783. JSTOR, JSTOR, [www.jstor.org/stable/1311183](http://www.jstor.org/stable/1311183).

30. Bergman, Christine, et al. "What Is Next for the Dietary Reference Intakes for Bone Metabolism Related Nutrients Beyond Calcium: Phosphorus, Magnesium, Vitamin D, and Fluoride?" *Critical Reviews in Food Science and Nutrition*, vol. 49, no. 2, 2009, pp. 136–144., doi:10.1080/10408390701764468.
31. Bronner, Felix, et al. *Bone Resorption*. Springer, 2005.
32. Frost HM: A 2003 update of bone physiology and Wolff's Law for clinicians. *Angle Orthod*, 2004, 74: 3–15. [PubMed]
33. "Wolff's law." Oxford Reference. 2007-01-01. . Date of access 7 Mar. 2018, <http://www.oxfordreference.com/view/10.1093/oi/authority.20110803124341929>
34. "Jubb, Kennedy & Palmer's Pathology of Domestic Animals: Volume 3." 2016, pp. 16–163., doi:10.1016/c2012-0-00792-2.
35. Ruff, Christopher, et al. "Who's Afraid of the Big Bad Wolff?: "Wolff's Law" and Bone Functional Adaptation." *American Journal of Physical Anthropology*, vol. 129, no. 4, 2006, pp. 484–498., doi:10.1002/ajpa.20371.
36. Biswas, Abhijit, et al. "Vibrotactile Sensitivity Threshold: Nonlinear Stochastic Mechanotransduction Model of the Pacinian Corpuscle." *IEEE Transactions on Haptics*, vol. 8, no. 1, 2015, pp. 102–113., doi:10.1109/toh.2014.2369422.
37. Katsumi, Akira, et al. "Integrins in Mechanotransduction." *Journal of Biological Chemistry*, vol. 279, no. 13, 2004, pp. 12001–12004., doi:10.1074/jbc.r300038200.
38. Sunter A, Armstrong VJ, Zaman G, et al. Mechano-transduction in Osteoblastic Cells Involves Strain-regulated Estrogen Receptor  $\alpha$ -mediated Control of Insulin-like Growth Factor (IGF) I Receptor Sensitivity to Ambient IGF, Leading to Phosphatidylinositol 3-Kinase/AKT-dependent Wnt/LRP5 Receptor-independent Activation of  $\beta$ -Catenin Signaling. *The Journal of Biological Chemistry*. 2010;285(12):8743-8758. doi:10.1074/jbc.M109.027086.
39. Rubin, Clinton T., and Lance E. Lanyon. "Dynamic Strain Similarity in Vertebrates; an Alternative to Allometric Limb Bone Scaling." *Journal of Theoretical Biology*, vol. 107, no. 2, 1984, pp. 321–327., doi:10.1016/s0022-5193(84)80031-4.
40. Turner, Charles H. "On Wolff's Law of Trabecular Architecture." *Journal of Biomechanics*, vol. 25, no. 1, 1992, pp. 1–9., doi:10.1016/0021-9290(92)90240-2.
41. Tsubota, Ken-Ichi, et al. "Computer Simulation of Trabecular Remodeling in Human Proximal Femur Using Large-Scale Voxel FE Models: Approach to Understanding Wolff's Law." *Journal of Biomechanics*, vol. 42, no. 8, 2009, pp. 1088–1094., doi:10.1016/j.jbiomech.2009.02.030.
42. Cowin, S. C., et al. "An Evolutionary Wolff's Law for Trabecular Architecture." *Journal of Biomechanical Engineering*, vol. 114, no. 1, 1992, p. 129., doi:10.1115/1.2895436.

43. Jang, In Gwon, and Il Yong Kim. "Computational Study of Wolff's Law with Trabecular Architecture in the Human Proximal Femur Using Topology Optimization." *Journal of Biomechanics*, vol. 41, no. 11, 2008, pp. 2353–2361., doi:10.1016/j.jbiomech.2008.05.037.
44. Jee, W. S., et al. "Effects of Spaceflight on Trabecular Bone in Rats." *American Journal of Physiology-Regulatory, Integrative and Comparative Physiology*, vol. 244, no. 3, 1983, doi:10.1152/ajpregu.1983.244.3.r310.
45. Goldstein, S.A., The mechanical properties of trabecular bone: dependence on anatomic location and function. *J Biomech*, 1987. 20(11-12): p. 1055-61.
46. Gibson, L.J., *Biomechanics of cellular solids*. *J Biomech*, 2005. 38(3): p. 377-99.
47. Ashby, M.F., The properties of foams and lattices. *Philos Trans A Math Phys Eng Sci*, 2006. 364(1838): p. 15-30.
48. Burr, David B., et al. "Bone Remodeling in Response to in Vivo Fatigue Microdamage." *Journal of Biomechanics*, vol. 18, no. 3, 1985, pp. 189–200., doi:10.1016/0021-9290(85)90204-0.
49. Liu, Xiaowei S, et al. "Quantification of the Roles of Trabecular Microarchitecture and Trabecular Type in Determining the Elastic Modulus of Human Trabecular Bone." *Journal of Bone and Mineral Research*, vol. 21, no. 10, 2006, pp. 1608–1617., doi:10.1359/jbmr.060716.
50. Rietbergen, B. Van, et al. "Relationships between Bone Morphology and Bone Elastic Properties Can Be Accurately Quantified Using High-Resolution Computer Reconstructions." *Journal of Orthopaedic Research*, vol. 16, no. 1, 1998, pp. 23–28., doi:10.1002/jor.1100160105.
51. Zysset, P.k., et al. "Morphology-Mechanical Property Relations in Trabecular Bone of the Osteoarthritic Proximal Tibia." *The Journal of Arthroplasty*, vol. 9, no. 2, 1994, pp. 203–216., doi:10.1016/0883-5403(94)90070-1.
52. Fyhrie, D. P., and D. R. Carter. "A Unifying Principle Relating Stress to Trabecular Bone Morphology." *Journal of Orthopaedic Research*, vol. 4, no. 3, 1986, pp. 304–317., doi:10.1002/jor.1100040307.
53. Zysset, P. K., et al. "A Global Relationship Between Trabecular Bone Morphology and Homogenized Elastic Properties." *Journal of Biomechanical Engineering*, vol. 120, no. 5, 1998, p. 640., doi:10.1115/1.2834756.
54. "Morphology." Merriam-Webster.com. Merriam-Webster, n.d. Web. 7 Mar. 2018.
55. Barak, Meir Max, Daniel E. Lieberman, and Jean-Jacques Hublin. "Of mice, rats and men: trabecular bone architecture in mammals scales to body mass with negative allometry." *Journal of structural biology* 183.2 (2013): 123-131.
56. Huayue Chen, Xiangrong Zhou, Hiroshi Fujita, Minoru Onozuka, and Kin-Ya Kubo, "Age-Related Changes in Trabecular and Cortical Bone Microstructure," *International Journal of Endocrinology*, vol. 2013, Article ID 213234, 9 pages, 2013. doi:10.1155/2013/213234

57. Legrand, Erick, et al. "Trabecular Bone Microarchitecture, Bone Mineral Density, and Vertebral Fractures in Male Osteoporosis." *Journal of Bone and Mineral Research*, vol. 15, no. 1, 2000, pp. 13–19., doi:10.1359/jbmr.2000.15.1.13.
58. Liu, X Sherry, et al. "Complete Volumetric Decomposition of Individual Trabecular Plates and Rods and Its Morphological Correlations With Anisotropic Elastic Moduli in Human Trabecular Bone." *Journal of Bone and Mineral Research*, vol. 23, no. 2, 2007, pp. 223–235., doi:10.1359/jbmr.071009.
59. Currey, J.D., Mechanical properties of bone tissues with greatly differing functions. *J Biomech*, 1979. 12(4): p. 313-9.
60. Mcgee-Lawrence, Meghan E., et al. "Grizzly Bears (*Ursus Arctos Horribilis*) and Black Bears (*Ursus Americanus*) Prevent Trabecular Bone Loss during Disuse (Hibernation)." *Bone*, vol. 45, no. 6, 2009, pp. 1186–1191., doi:10.1016/j.bone.2009.08.011.
61. Kurtén, Björn. *The Cave Bear Story: Life and Death of a Vanished Animal*. Columbia University Press, 1995.
62. Stiller, M., et al. "Withering Away--25,000 Years of Genetic Decline Preceded Cave Bear Extinction." *Molecular Biology and Evolution*, vol. 27, no. 5, 2010, pp. 975–978., doi:10.1093/molbev/msq083.
63. Chinsamy-Turan, Anusuya. *The microstructure of dinosaur bone: deciphering biology with fine-scale techniques*. John Wiley & Sons, 2005.
64. Christiansen, Per. "What size were *Arctodus simus* and *Ursus spelaeus* (Carnivora: Ursidae)?" *Annales Zoologici Fennici*. Finnish Zoological and Botanical Publishing Board, 1999.
65. Blanchard, Bonnie M. "Size and growth patterns of the Yellowstone grizzly bear." *Bears: Their Biology and Management* (1987): 99-107.
66. Bates, Karl T., et al. "Estimating mass properties of dinosaurs using laser imaging and 3D computer modelling." *PLoS One* 4.2 (2009): e4532.
67. "Hadrosaurs." *Hadrosaurs*, by David A. Eberth et al., Indiana University Press, 2014, pp. 239–241.
68. Hutchinson, John R., and Mariano Garcia. "Tyrannosaurus was not a fast runner." *Nature* 415.6875 (2002): 1018.
69. Alexander, R. McNeill. "Dinosaur biomechanics." *Proceedings of the Royal Society of London B: Biological Sciences* 273.1596 (2006): 1849-1855.
70. Sellers, William Irvin, et al. "March of the titans: the locomotor capabilities of sauropod dinosaurs." *PloS one* 8.10 (2013): e78733.
71. Tombolato, L., et al., Microstructure, elastic properties and deformation mechanisms of horn keratin. *Acta Biomater*, 2010. 6(2): p. 319-30.

72. McKittrick, J., et al., The Structure, Functions, and Mechanical Properties of Keratin. *Jom*, 2012. 64(4): p. 449-468.
73. McKittrick, J., et al., Energy absorbent natural materials and bioinspired design strategies: A review. *Materials Science & Engineering C-Materials for Biological Applications*, 2010. 30(3): p. 331-342.
74. Trim, M.W., et al., The effects of water and microstructure on the mechanical properties of bighorn sheep (*Ovis canadensis*) horn keratin. *Acta Biomater*, 2011. 7(3): p. 1228-40.
75. Kitchener, A., An Analysis of the Forces of Fighting of the Blackbuck (*Antelope-Cervicapra*) and the Bighorn Sheep (*Ovis-Canadensis*) and the Mechanical Design of the Horns of Bovids. *Journal of Zoology*, 1988. 214: p. 1-20.
76. Kitchener, A., Fracture-Toughness of Horns and a Reinterpretation of the Horning Behavior of Bovids. *Journal of Zoology*, 1987. 213: p. 621-639.
77. Drake, A., et al., Horn and horn core trabecular bone of bighorn sheep rams absorbs impact energy and reduces brain cavity accelerations during high impact ramming of the skull. *Acta Biomater*, 2016. 44: p. 41-50.
78. Hunter, Allison K., and W. D. McDavid. "Characterization and correction of cupping effect artefacts in cone beam CT." *Dentomaxillofacial Radiology* 41.3 (2012): 217-223.
79. Hildebrand, Tor, and Peter Rügsegger. "A new method for the model-independent assessment of thickness in three-dimensional images." *Journal of microscopy* 185.1 (1997): 67-75.
80. Hildebrand, Tor, et al. "Direct three-dimensional morphometric analysis of human cancellous bone: microstructural data from spine, femur, iliac crest, and calcaneus." *Journal of bone and mineral research* 14.7 (1999): 1167-1174.
81. Doube, Michael, et al. "Trabecular bone scales allometrically in mammals and birds." *Proceedings of the Royal Society of London B: Biological Sciences* (2011): rspb20110069.
82. Kadir, Mohammed Rafiq Abdul, Ardiyansyah Syahrom, and Andreas Öchsner. "Finite element analysis of idealised unit cell cancellous structure based on morphological indices of cancellous bone." *Medical & biological engineering & computing* 48.5 (2010): 497-505.